Optimum Reconfigurable Intelligent Surface Selection for Wireless Networks

Yuting Fang, *Member, IEEE*, Saman Atapattu, *Senior Member, IEEE*,

Hazer Inaltekin, *Member, IEEE*, and Jamie Evans, *Senior Member, IEEE*

Abstract

The reconfigurable intelligent surface (RIS) is a promising technology that is anticipated to enable high spectrum and energy efficiencies in future wireless communication networks. This paper investigates optimum location-based RIS selection policies in RIS-aided wireless networks to maximize the end-to-end signal-to-noise ratio for product-scaling and sum-scaling path-loss models where the received power scales with the *product* and *sum* of the transmitter-to-RIS and RIS-to-receiver distances, respectively. These scaling laws cover the important cases of end-to-end path-loss models in RIS-aided wireless systems. The random locations of all available RISs are modeled as a Poisson point process. To quantify the network performance, the outage probabilities and average rates attained by the proposed RIS selection policies are evaluated by deriving the distance distribution of the chosen RIS node as per the selection policies for both product-scaling and sum-scaling path-loss models. We also propose a limited-feedback RIS selection framework to achieve distributed network operation. The outage probabilities and average rates obtained by the limited-feedback RIS selection policies are derived for both path-loss models as well. The numerical results show notable performance gains obtained by the proposed RIS selection policies.

Index Terms

Poisson point process (PPP), reconfigurable intelligent surface (RIS), stochastic geometry.

I. Introduction

A. Background and Motivation

Globally, mobile and machine-to-machine data traffic is expected to grow at a rate of about 55% per year from 2020 to 2030, reaching 5,000 Exabytes per month in 2030 [1]. While supporting 1 Terabyte per second speeds, the sixth-generation (6G) wireless networks are expected to facilitate sensing, localization, and computing in real-time by using a smart wireless environment. One of the key enablers to realizing a smart environment is a reconfigurable intelligent surface (RIS), which includes many nearly passive elements having ultra-low power consumption. Each element can electronically control the phase of the reflected radio waves to concentrate energy in the desired spatial directions [2]. As such, an RIS dynamically adapts to changing wireless channel conditions to create a favorable

propagation environment and to increase the energy efficiency of wireless networks [3]. Moreover, RIS greatly decreases hardware costs and power consumption. This is because the spatial feeding method of the RIS avoids the immoderate power loss due to the massive feeding networks of phased arrays [4]. A critical milestone to realize the full scale of these advantages in a network setting is to have adaptive algorithms optimizing the selection and activation of RISs to enhance smart wireless connectivity, which will be an essential feature of future wireless systems.

Due to the possible irregular terrain for deployment of RISs, it is naturally expected that multiple RISs will be deployed according to a potentially random-looking topology to provide connectivity in future wireless networks. In these cases, the best RISs will need to be selected for achieving high quality connection between given source and destination nodes, in contrast to popular single and fixed RIS deployments. Similar to relay networks, utilizing multiple RISs for single-user communication increases the overall system complexity and signaling overhead. Thus, a well-designed adaptive RIS-selection policy is of particular importance to achieve the benefits of the multiple RIS deployment topologies. Further, RISs are proposed to be nearly passive network elements with limited computing power to support signal processing and edge computing. Therefore, a selection policy utilizing only location information of available RISs is more practical in this context, which can be assumed to be time-invariant. Motivated by these facts, this paper aims to focus on the location-based optimum RIS selection problem in RIS-aided future wireless networks that consist of multiple randomly distributed RISs and derives performance metrics under the optimum selection policy.

B. Related Work

Most previous work on performance analysis of RIS-aided wireless communications considers different wireless network scenarios with single and fixed RIS setup, e.g., [5], [6]. [7]–[14] considers a given set of locations of multiple RISs without RIS selection. Specifically, the signal-to-noise ratio (SNR), achievable sum-rate, secrecy rate, and energy efficiency of RIS-assisted networks are maximized in [7]–[10], respectively. [11] proposes and analyzes a double-RIS aided system. [12] investigates the capacity region of a two-user network with one access point aided by multiple RIS elements. [13] proposes a channel estimation framework for a RIS-aided multi-user system. [14] designs a novel hybrid beamforming scheme for a RIS-aided multi-hop network. Very recently, the RIS-user associations with and without the BS power control are optimized in a multi-RIS aided network in [15]. The RIS with the highest instantaneous end-to-end SNR is selected among multiple fixed RISs to aid the communication in [16], where the outage probability and average sum-rate are

investigated. This paper only focuses on deterministic RIS deployment without modeling potential randomness in RIS locations.

Spatial point processes are regarded as tractable analytical tools to model the locations of the network elements (e.g., base stations, users, or relays), with a good statistical fit to physical wireless network deployments [17]. However, only a few papers have so far focused on spatial network models for the deployment of RISs or the distribution of users in RIS-assisted networks; see [18]–[23]. In [18], environmental objects are assumed to be coated as RISs where the deployment is modeled as a modified line process with random locations and orientations. In [19], they propose a joint design for the detection weight at randomly distributed users and passive beamforming weight at RISs. [20] considers a cellular network where the midpoints of the blockages are distributed according to a Poisson point process (PPP) and the blockages are equipped with RISs. [21] provides performance analysis of a large-scale mmWave cellular network where the locations of base stations and RISs are modeled using independent PPPs. Recently, [22] studies the coverage of an RIS-aided large-scale mmWave cellular network where the buildings with RISs are distributed according to a PPP. [23] analyzes the coverage probability, ergodic capacity, and energy efficiency for indirect RIS-aided network with where the locations of the RISs follow a binomial point process. Very recently, [24] analyzes the outage probability of an RIS-aided network where multiple IRSs are randomly distributed with different association policies activating a random RIS, the closest RIS to the transmitter, or all available RISs. However, none of these papers considered a selection strategy choosing the best RIS from a collection of randomly distributed RISs to optimize connectivity between source and destination nodes. Performance characterization of RIS-aided random wireless networks with such optimum RIS selection is an open problem in the literature, which we tackle in this paper.

C. Our Approach and Contributions

In this paper, we consider an RIS-aided wireless network where multiple RISs are randomly distributed and an RIS is optimally selected to assist data transmission from a transmitter (TX) to a receiver (RX) based on the relative locations of RISs with respect to TX and RX nodes. As analyzed in [25]–[27], the scaling law of received power through the reflection of an RIS is a function of the TX-RIS and RIS-RX distances. We note that the product-scaling law where the path-loss scales according to the *product* of the TX-RIS and RIS-RX distances and the sum-scaling law where the path-loss scales according to the *sum* of these distances have been established as the fundamental path-loss models to model the end-to-end signal power attenuation when the TX and RX nodes are connected by an intermediate RIS. They will be the path-loss models that we follow in this paper. Using the tools from

stochastic geometry, we develop a tractable theoretical framework to obtain the outage probability and average rate for the RIS-aided wireless network under the optimum RIS selection policies for both path-loss scaling laws. We also analyze the limited feedback case to achieve distributed network operation under the assumption of availability of RIS feedback capability for selection. We emphasize that the derivations of our theoretical results are challenging since we need to tackle the *random* instantaneous SNR values at the random RIS locations coupled with the *randomness* over the fading process. Despite these challenges, we make the following novel contributions:

- Based on the nature of the SNR in RIS-aided wireless networks, we propose location-based optimum RIS selection policies that maximize the end-to-end SNR of the link connecting a TX and a RX via an RIS for product-scaling and sum-scaling path-loss models. These selection policies make RIS selection decisions based on the insight that the optimum RIS given the *product-scaling* path-loss law is the RIS that has the *minimal product* of the distances of the TX-RIS and RIS-RX links among all randomly distributed RISs. On the other hand, the optimum RIS given the *sum-scaling* path-loss law is the RIS that has the *minimal sum* of these distances.

- We derive the distance distribution of the optimum RIS node for both path-loss models. These distributions are of critical importance to obtain the outage probability of RIS-aided wireless networks. The derived distributions have broader applicability where a node that has the minimal product or sum of the distances is selected. Using the derived distance distribution and the gamma approximation for fading channels, we derive theoretical expressions for the outage probability and average rate of the optimum RIS selection policies for product-scaling and sum-scaling path-loss models.

- To characterize the system performance given limited-feedback RIS selection policy, we derive the average number of RISs feeding back and confirm the number of RISs feeding back is a Poisson random variable (RV) for both path-loss models. Using this result, we obtain theoretical expressions for the outage probability and average rate under the limited-feedback RIS selection policies for both path-loss models.

We verify the derived analytical results by means of extensive numerical analysis and simulations. The potential performance improvement obtained by the optimum RIS selection policy is demonstrated by comparing the performance gains obtained by the optimum policy with those of heuristic sub-optimum policies via simulations. Our results reveal that a selection policy performing optimally for decode-and-forward (DF) relay networks (i.e., the min-max policy) can perform very poorly for RIS networks due to fundamentally different signal propagation characteristics. From a system
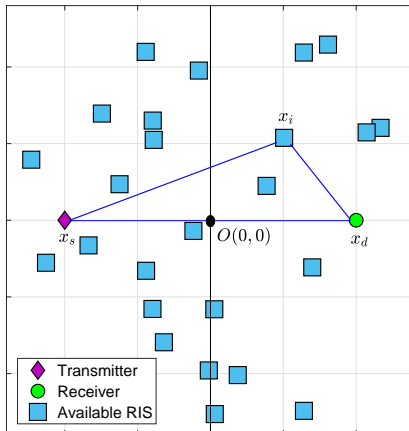
Fig. 1: An example illustration for an RIS-aided wireless network.

design point of view, this is an important result. Numerical results also demonstrate that limited-feedback RIS selection policies achieve almost the same outage and data rate performance as the optimum centralized RIS selection policy while significantly reducing the feedback and signaling load. Through these theoretical and numerical results, this paper provides important guidelines for selecting the optimal RIS towards a reliable yet practical RIS-aided wireless network.

The results in [28] focus on the node distance distribution given the min-max optimum selection criteria, and cannot be directly applied to this paper. Our key technical challenges are to solve the node distance distribution given the min-product and min-sum optimum selection criteria. These are fundamentally different problems with their own particular technical challenges requiring new solution approaches when compared to those investigated in [28]. Moreover, there are also fundamental differences between RIS-aided networks and relay-aided networks in terms of their end-to-end path-loss scaling laws as a function of the TX-to-RIS and RIS-to-RX distances; see [25], [29]. Thus, this paper provides novel theoretical results and numerical insights that have not been studied before.

D. Notation

We use boldface letters to represent vector quantities. $\mathbb{N}$ denotes the set of natural numbers and $\mathbb{R}^2$ denotes the two-dimensional Euclidean space. $|x|$ and $\|\boldsymbol{x}\|$ denote the absolute value of a scalar quantity x (real or complex) and the Euclidean norm of a vector quantity $\boldsymbol{x}$, respectively. $\mathbb{P}(\cdot)$ denotes probability. $\mathsf{E}_Z[\cdot]$ is the expectation over RV Z. $\mathsf{E}_\Phi[\cdot]$ is the expectation over the point process Φ.

II. SYSTEM AND ANALYTICAL MODELS

A. System Model

We consider an RIS-aided wireless system in $\mathbb{R}^2$, as illustrated in Fig. 1, where the TX and RX are located at arbitrary locations, denoted by $\boldsymbol{x}_{\mathrm{s}} \in \mathbb{R}^2$ and $\boldsymbol{x}_{\mathrm{d}} \in \mathbb{R}^2$, respectively. Potential RISs are

randomly distributed according to a spatial homogeneous Poisson point process (PPP) Φ with density $\lambda > 0$. The locations of available RISs are denoted by $\phi = \{\boldsymbol{x}_1, \boldsymbol{x}_2, \ldots\}$, where $\boldsymbol{x}_i \in \mathbb{R}^2$ is the ith RIS location for $i \in \mathbb{N}$ and ϕ is a particular realization of $\Phi = \{\boldsymbol{X}_1, \boldsymbol{X}_2, \ldots\}$. We consider that the locations of available RISs are known by a central network controller to make a decision for selecting an RIS to aid the communication between the TX and RX[1]. As in [15], [24], we assume when one RIS is selected (activated), the remaining RISs remain switched off. We assume the signal power received over the longer TX-RX link is much smaller than the one received over the shorter RIS-RX link, i.e., there is no direct link between TX and RX[2].

We assume nearly passive RISs as introduced in [25] where each RIS is implemented with N number of reflecting elements which can be adjusted individually for adapting to fading conditions. We denote $\mathcal{W} = \text{diag}\left(\exp\left(j\varpi_{i,1}\right), \ldots, \exp\left(j\varpi_{i,N}\right)\right)$ as phase shifts of the ith RIS. Further, we denote $h_{i,n} = \alpha_{i,n}\exp(-j\psi_{i,n})$ and $g_{i,n} = \beta_{i,n}\exp(-j\varphi_{i,n})$ as fading channels between the TX and the nth reflecting element of the ith RIS and that between the nth reflecting element of the ith RIS and the RX, respectively. As in [29], [30], we assume $h_{i,n}$ and $g_{i,n}$ are independent and identically distributed (i.i.d.) complex Gaussian RVs with zero mean and unit variance i.e., $h_{i,n}, g_{i,n} \sim \mathcal{CN}(0,1)$. Hence, magnitudes $\alpha_{i,n}$ and $\beta_{i,n}$ follow the Rayleigh distribution. Then, the instantaneous received signal[3] at time t via the ith RIS located at $\boldsymbol{X}_i$ is given by [30, eq. (11)]

$$y_i(t) = \frac{\sqrt{P}\sum_{n=1}^{N}\alpha_{i,n}\beta_{i,n}\exp(j(\varpi_{i,n} - \psi_{i,n} - \varphi_{i,n}))}{\sqrt{G\left(\|\boldsymbol{x}_{\text{s}} - \boldsymbol{X}_i\|, \|\boldsymbol{X}_i - \boldsymbol{x}_{\text{d}}\|\right)}}s(t) + w(t), \tag{1}$$

where P denotes the transmit power, $s(t)$ is a unit energy signal, $w(t)$ is additive white Gaussian noise (AWGN) having complex Gaussian distribution with mean zero and variance N_0. $G\left(\|\boldsymbol{x}_{\text{s}} - \boldsymbol{X}_i\|, \|\boldsymbol{X}_i - \boldsymbol{x}_{\text{d}}\|\right)$ is a path-loss function and we will discuss its dependence on the TX-RIS distance $\|\boldsymbol{x}_{\text{s}} - \boldsymbol{X}_i\|$ and the RIS-RX distance $\|\boldsymbol{X}_i - \boldsymbol{x}_{\text{d}}\|$ in Sec. II-B. A careful inspection of the structure of (1) reveals that the optimal choice of $\varpi_{i,n}$ that maximizes the instantaneous received signal $y_i(t)$ is $\varpi_{i,n} = \psi_{i,n} + \varphi_{i,n}, i \in \mathbb{N}$. This is feasible at RISs since they can obtain the knowledge of the channel phases by various methods mentioned in [2], [30], [32], e.g., by embedding low-power sensors

---

[1]Our system setup can be applied in the scenarios where RISs are irregularly deployed and one RIS is selected to enhance the communication from the source to destination. For example, in a RIS-enhanced cellular network, potential RISs are employed on irregularly-located trees or buildings and the optimal RIS is selected to strengthen the received signal power of a cell-edge user.

[2]This assumption is reasonable when the direct link is severely shadowed by an object in the environment or the decay of path-loss with distance is very sharp.

[3]In practice, the obliquity factor (i.e., the incidence and reflected angles of signals at the RIS) mentioned in [31] and blockages may affect the power received at the RX via the RIS. For tractability, as in [16], [19], [23], we ignore the obliquity factor and blockages when modeling the received power via the RIS.

throughout the RISs. Thus, the assumption of optimal phase shifting is widely adopted in existing RIS studies, e.g., [29], [30], [33], [34]. Using this assumption, (1) can be rewritten as

$$y_i(t) = \frac{\sqrt{P}Z_i}{\sqrt{G\left(\|\boldsymbol{x}_\mathrm{s} - \boldsymbol{X}_i\|, \|\boldsymbol{X}_i - \boldsymbol{x}_\mathrm{d}\|\right)}}s(t) + w(t), \tag{2}$$

where $Z_i = \sum_{n=1}^{N} \alpha_{i,n}\beta_{i,n}$. We note that Z_i are i.i.d. RVs for different RISs. Thus, for compactness, we remove subscript "i" from Z_i, i.e., $Z_i = Z, \forall i$, in the rest of the paper, and it will be clear from the context that Z is the power gain associated with the RIS selected to connect TX and RX.

B. RIS Selection Policies

In this subsection, we first give the instantaneous SNR of an RIS-aided wireless network, then discuss the path-loss scaling laws, and finally formulate the location-based optimum RIS selection policies that maximize the instantaneous SNR for different path-loss scaling laws.

We consider the case where a single RIS is selected for aiding the communication between the TX and RX according to a given RIS selection policy which is defined as follows:

Definition 1: an RIS selection policy $\mathcal{P} : \Sigma \mapsto \mathbb{R}^2$ is a mapping from the set of all countable locally finite subsets of $\mathbb{R}^2$, denoted by Σ, to $\mathbb{R}^2$, that satisfies the condition $\mathcal{P}(\phi) \in \phi$ for all $\phi \in \Sigma$.

With a slight abuse of notation, we will denote the RIS selected by $\mathcal{P}$ as $\boldsymbol{X}_\mathcal{P}$. Using (2), we write the instantaneous SNR associated with RIS $\boldsymbol{X}_\mathcal{P}$ according to

$$\mathsf{SNR}_\mathrm{inst}\left(\mathcal{P}, \Phi, Z\right) = \frac{\bar{\gamma}Z^2}{G(\|\boldsymbol{x}_\mathrm{s} - \boldsymbol{X}_\mathcal{P}\|, \|\boldsymbol{X}_\mathcal{P} - \boldsymbol{x}_\mathrm{d}\|)}, \tag{3}$$

where $\bar{\gamma} = \frac{P}{N_0}$ is the average SNR.

We next discuss the dependence of a path-loss function $G(\|\boldsymbol{x}_\mathrm{s} - \boldsymbol{X}_\mathcal{P}\|, \|\boldsymbol{X}_\mathcal{P} - \boldsymbol{x}_\mathrm{d}\|)$ on the TX-RIS distance $\|\boldsymbol{x}_\mathrm{s} - \boldsymbol{X}_\mathcal{P}\|$ and the RIS-RX distance $\|\boldsymbol{X}_\mathcal{P} - \boldsymbol{x}_\mathrm{d}\|$. Based on [25]–[27], [31], the scaling law of the end-to-end received power through the reflection of an RIS as a function of the TX-RIS and RIS-RX distances, depends on the relation between the geometric size of the RIS, the wavelength of the radio wave, and the relative TX-RIS and RIS-RX distances. Notably, two path-loss scaling laws of the TX-RIS and RIS-RX distances are worth of analysis.

1) Product-Scaling path-loss models: If the size of the RIS is not large enough as compared with the wavelength and the transmission distances $\|\boldsymbol{x}_\mathrm{s} - \boldsymbol{X}_\mathcal{P}\|$ and $\|\boldsymbol{X}_\mathcal{P} - \boldsymbol{x}_\mathrm{d}\|$, the end-to-end received power at the receiver scales, as $4L_1^2(\|\boldsymbol{x}_\mathrm{s} - \boldsymbol{X}_\mathcal{P}\| \|\boldsymbol{X}_\mathcal{P} - \boldsymbol{x}_\mathrm{d}\|)$ [27], where $2L_1$ is the length of one-dimensional RIS. [26] also gives similar scaling laws[4] with different power of product distances

---

[4]For example, in [26], a large RIS with the size of $1\,\mathrm{m} \times 1.2\,\mathrm{m}$ and the carrier frequency of $10.5\,\mathrm{GHz}$ at the TX-RIS distance of $100\,\mathrm{m}$ and the RIS-RX distance of $100\,\mathrm{m}$ and a small RIS with the size of $0.384\,\mathrm{m} \times 0.096\,\mathrm{m}$ and the carrier frequency of $4.25\,\mathrm{GHz}$ at the TX-RIS distance of $3.5\,\mathrm{m}$ and the RIS-RX distance of $10\,\mathrm{m}$ are shown to operate as the product-scaling path-loss model.

in the far-field case[5], where the path loss of through the reflection of an RIS is proportional to $(\|\boldsymbol{x}_{\mathrm{s}} - \boldsymbol{X}_{\mathcal{P}}\| \|\boldsymbol{X}_{\mathcal{P}} - \boldsymbol{x}_{\mathrm{d}}\|)^2$. The path-loss given in [26] also relates to the antenna gains, the RIS element gain, and other system parameters. Moreover, [31] shows for focusing lenses of RISs, a single scaling law is observed, i.e., the product path-loss model is *sufficiently accurate for short and long distances*. On the other hand, for a classical power-law path-loss model, signal power decays as $G^{\mathrm{pow}}(d) = d^{\eta}$, where d is the link distance and $\eta > 2$ is the path-loss exponent. The end-to-end path-loss for the power-law model is $G^{\mathrm{pow}}(\|\boldsymbol{x}_{\mathrm{s}} - \boldsymbol{X}_{\mathcal{P}}\|, \|\boldsymbol{X}_{\mathcal{P}} - \boldsymbol{x}_{\mathrm{d}}\|) = (\|\boldsymbol{x}_{\mathrm{s}} - \boldsymbol{X}_{\mathcal{P}}\| \|\boldsymbol{X}_{\mathcal{P}} - \boldsymbol{x}_{\mathrm{d}}\|)^{\eta}$. Overall, the end-to-end path-loss for all aforementioned cases is proportional to the *product of the distances between TX-RIS and RIS-RX*, although being with different exact path-loss expressions. Our key analytical results below will hold for all path-loss functions resulting in product-scaling for the end-to-end SNR achieved via an intermediate RIS. For performance evaluation, we will consider a specific product-scaling path-loss model.

2) Sum-Scaling path-loss models: If the geometric size of the RIS is large enough as compared with the wavelength λ_s and the transmission distances $\|\boldsymbol{x}_{\mathrm{s}} - \boldsymbol{X}_{\mathcal{P}}\|$ and $\|\boldsymbol{X}_{\mathcal{P}} - \boldsymbol{x}_{\mathrm{d}}\|$, the end-to-end received power scales according to $(\mu k \|\boldsymbol{x}_{\mathrm{s}} - \boldsymbol{X}_{\mathcal{P}}\| + \nu k \|\boldsymbol{X}_{\mathcal{P}} - \boldsymbol{x}_{\mathrm{d}}\|)$, where $k = \frac{2\pi}{\lambda_s}$ and the coefficients μ and ν depend on the angles of incidence and reflection of the radio waves [25], [27]. Further, [26] also empirically validates that the path-loss function G, when the TX and RX both or only one of them are in the near-field of RIS[6], is approximately proportional to $(\|\boldsymbol{x}_{\mathrm{s}} - \boldsymbol{X}_{\mathcal{P}}\| + \|\boldsymbol{X}_{\mathcal{P}} - \boldsymbol{x}_{\mathrm{d}}\|)^2$. G in this particular case depends on antenna gains, wavelength, and the amplitude value of RIS elements as well. Also, for the exponential-law path-loss model, which we refer to as exp-law for brevity for the rest of the paper, signal power decays over a link as $G^{\mathrm{exp}}(d) = \exp(\alpha d^{\beta})$, where $\alpha > 0$ and $\beta > 0$ are tunable parameters [35]. We note that the exp-law model is suitable for modeling short-range communication, e.g., indoor communication[7], which is one of the important scenarios that RISs can be deployed to assist communications. For $\beta = 1$[8], the exp-law path-loss model can be expressed as $G^{\mathrm{exp}}(\|\boldsymbol{x}_{\mathrm{s}} - \boldsymbol{X}_{\mathcal{P}}\|, \|\boldsymbol{X}_{\mathcal{P}} - \boldsymbol{x}_{\mathrm{d}}\|) = \exp\left(\alpha\left(\|\boldsymbol{x}_{\mathrm{s}} - \boldsymbol{X}_{\mathcal{P}}\| + \|\boldsymbol{X}_{\mathcal{P}} - \boldsymbol{x}_{\mathrm{d}}\|\right)\right)$. In the cases

---

[5]When the distance between the TX(RX) and the center of the RIS is less than $\xi = \frac{2D^2}{\lambda_s}$, the RIS is considered to be in the near-field of the TX(RX). Otherwise, the RIS is said to be in the far-field of the TX(RX).

[6]For example, a RIS prototype in [26], whose size is $0.34\,\mathrm{m} \times 0.5\,\mathrm{m}$ and whose carrier frequency is 10.5 GHz, at the TX-RIS distance of $0.5\,\mathrm{m}$ and the RIS-RX distance of $1\,\mathrm{m}$ is shown to operate as the sum-scaling path-loss model.

[7]For indoor environments, mmWave transmissions would be more appropriate due to having shorter transmission distances. Hence, the RIS size can be considered as large when compared to the transmission wavelength for indoor environments.

[8]$\beta = 1$ suits for indoor communications when the number of obstacles scales linearly with the distance of the link between $\boldsymbol{x}_{\mathrm{s}}$ and $\boldsymbol{X}_{\mathcal{P}}$ and the one between $\boldsymbol{X}_{\mathcal{P}}$ and $\boldsymbol{x}_{\mathrm{d}}$.

mentioned above, we note that the path-loss function G scales with *the sum of the distance between TX-RIS and RIS-RX* and our results below hold correct for such cases.

Due to the random locations of RISs in a PPP, the TX-RIS and RIS-RX distances are random. Thus, RISs in a PPP may be in the regime where the product-scaling law holds or the regime where the sum-scaling law holds. We note that considering mixture path-loss models (e.g., product-scaling, sum-scaling, or other models which do not directly depend on distances) for potential RISs and analytically deriving the performance metrics of corresponding optimum selection policies is important future work. For tractable performance analysis, we assume all RIS-aided links in a PPP have the product-scaling law or all RIS-aided links in a PPP have the sum-scaling law for solving the optimum RIS selection problems. We note that this assumptions is reasonable because in some cases, a single scaling law is accurate. For example, based on [31], for focusing lenses of RISs, a single product-scaling law is observed, and for anomalous reflectors, the sum-scaling law may be accurate up a few tens of meters. We also have conducted simulations with mixture path-loss models and compare these simulations with our analysis with a single path-loss model for all potential RISs, to show the feasibility of the assumption. The reasonableness is shown by the facts that i) the results derived by assuming all RISs have the sum-scaling law can be good approximations of the results that assumes the mixture product and sum scaling path-loss models for large RISs, and ii) the results assuming all RISs have the product-scaling path-loss model can be good approximations of the results assuming the mixture product and sum scaling path-loss models for small RISs. Our simulation results and detailed discussions are presented in Appendix D. Moreover, this assumption is widely used in the papers that consider random locations of RISs or users, e.g., [19], [20], [23], [24].

We can maximize the instantaneous SNR by selecting the RIS that has the *minimal product* of the distances of the TX-RIS and RIS-RX links over the set of RIS locations in Φ, when all available RIS-aided links follow product-scaling path-loss models (i.e., only the product-based path-loss scaling law is observed). Similarly, the optimum RIS that maximizes the instantaneous SNR for the sum-scaling path-loss model is the one that has the *minimal sum* of these distances, when all available RIS-aided links follow sum-scaling path-loss models (i.e., only the sum-based path-loss scaling law is observed). Thus, we can formulate the optimum RIS selection problem for the product-scaling path-loss model as follows:

$$\begin{aligned} \underset{\boldsymbol{X} \in \mathbb{R}^2}{\text{minimize}} \quad & \widehat{s}_{\text{pro}}\left(\boldsymbol{X}\right) \\ \text{subject to} \quad & \boldsymbol{X} \in \Phi \end{aligned}, \tag{4}$$

where $\widehat{s}_{\text{pro}}\left(\boldsymbol{X}\right)$ is given by $\widehat{s}_{\text{pro}}\left(\boldsymbol{X}\right) = \|\boldsymbol{x}_{\text{s}} - \boldsymbol{X}\| \times \|\boldsymbol{X} - \boldsymbol{x}_{\text{d}}\|$. With the aim of maximizing the

instantaneous SNR for the sum-scaling path-loss model, the optimum RIS selection problem can be formulated as:

$$\underset{\boldsymbol{X} \in \mathbb{R}^2}{\text{minimize}} \quad \widehat{s}_{\text{sum}}\left(\boldsymbol{X}\right)$$
$$\text{subject to} \quad \boldsymbol{X} \in \Phi \tag{5}$$

where $\widehat{s}_{\text{sum}}\left(\boldsymbol{X}\right)$ is given by $\widehat{s}_{\text{sum}}\left(\boldsymbol{X}\right) = \|\boldsymbol{x}_{\text{s}} - \boldsymbol{X}\| + \|\boldsymbol{X} - \boldsymbol{x}_{\text{d}}\|$. The corresponding optimum RIS selection policies for the product-scaling and sum-scaling path-loss models are formally defined as follows:

Selection Policy 1: The optimum RIS selection policy for the product-scaling path-loss law, denoted by $\mathcal{P}_{\text{pro}}^{*}$, is the one solving (4) for all realizations of Φ in Σ. The optimum RIS location maximizing the instantaneous SNR for the product-scaling path-loss law, $\boldsymbol{X}_{\times}^{*}$, is $\boldsymbol{X}_{\times}^{*} = \arg\min_{\boldsymbol{X} \in \Phi} \widehat{s}_{\text{pro}}\left(\boldsymbol{X}\right)$, which is unique with probability one.

Selection Policy 2: The optimum RIS selection policy under the sum-scaling path-loss law, denoted by $\mathcal{P}_{\text{sum}}^{*}$, is the one solving (5) for all realizations of Φ in Σ. The optimum RIS location to maximize the instantaneous SNR for the sum-scaling path-loss law, $\boldsymbol{X}_{+}^{*}$, is $\boldsymbol{X}_{+}^{*} = \arg\min_{\boldsymbol{X} \in \Phi} \widehat{s}_{\text{sum}}\left(\boldsymbol{X}\right)$, which is also unique with probability one.

C. Performance Metrics

In this paper, we aim to characterize the performance metrics associated with $\mathcal{P}_{\text{pro}}^{*}$ and $\mathcal{P}_{\text{sum}}^{*}$. To this end, we first define the performance metrics of a given RIS selection policy $\mathcal{P}$ in this subsection. We will use the averaged SNR to determine outage probability and data rate over the fading process to characterize the data performance of an RIS selection policy $\mathcal{P}$[9]. We use $\mathsf{E}_Z\left[\mathsf{SNR}_{\text{inst}}\left(\mathcal{P}, \Phi, Z\right)\right]$ and $\mathsf{E}_Z\left[\log_2\left(1 + \mathsf{SNR}_{\text{inst}}\left(\mathcal{P}, \Phi, Z\right)\right)\right]$ as the SNR and data rate averaged over the fading process, respectively. For compactness, we define $\mathsf{E}_Z\left[\mathsf{SNR}_{\text{inst}}\left(\mathcal{P}, \Phi, Z\right)\right] \triangleq \mathsf{SNR}\left(\mathcal{P}, \Phi\right)$ and $\mathsf{E}_Z\left[\log_2\left(1 + \mathsf{SNR}_{\text{inst}}\left(\mathcal{P}, \Phi, Z\right)\right)\right] \triangleq \mathsf{R}\left(\mathcal{P}, \Phi\right)$ in the rest of the paper. We note that $\mathsf{SNR}\left(\mathcal{P}, \Phi\right)$ and $\mathsf{R}\left(\mathcal{P}, \Phi\right)$ are still random quantities since they depend on random RIS locations. Using $\mathsf{SNR}\left(\mathcal{P}, \Phi\right)$, we define the outage probability as follows:

Definition 2: For a target SNR ρ, the SNR-outage probability $\mathsf{P}_{\text{out}}\left(\mathcal{P}\right)$ achieved by an RIS selection policy $\mathcal{P}$ is given by

$$\mathsf{P}_{\text{out}}\left(\mathcal{P}\right) = \Pr\left\{\mathsf{SNR}\left(\mathcal{P}, \Phi\right) \leq \rho\right\}. \tag{6}$$

Using $\mathsf{R}\left(\mathcal{P}, \Phi\right)$, we define the average rate as follows:

---

[9]These are relevant metrics when the permissible decoding delay is large enough to average over the fading process.

Definition 3: The average rate achieved by an RIS selection policy $\mathcal{P}$ is given by

$$R_{ave}(\mathcal{P}) = \mathsf{E}_\Phi[R(\mathcal{P}, \Phi)]. \tag{7}$$

In the next sections, we will evaluate P_{out} and R_{ave} for the optimum RIS selection policies $\mathcal{P}^*_{pro}$ and $\mathcal{P}^*_{sum}$. This is a challenging problem since we need to derive the distribution of optimum RIS distance functions $\widehat{s}_{pro}(\boldsymbol{X}^*_\times)$ and $\widehat{s}_{sum}(\boldsymbol{X}^*_+)$ over the random spatial point process Φ and the averaged performance metrics over the random fading process.

III. OPTIMUM RIS DISTANCE DISTRIBUTION AND PERFORMANCE ANALYSIS

In this section, we first obtain the optimum RIS distance distributions under the product-scaling and sum-scaling path-loss models. We second derive the averaged performance metrics over the fading process for general path-loss functions $G(\|\boldsymbol{x}_s - \boldsymbol{X}_\mathcal{P}\|, \|\boldsymbol{X}_\mathcal{P} - \boldsymbol{x}_d\|)$.

Using the optimum RIS distance distribution and the averaged performance metrics, we will evaluate the outage probability and average rate for the given optimum RIS selection policy under specific path-loss models. We note that there are multiple potential models for product-scaling and sum-scaling path-loss models, as discussed in Sec. II-B. For performance analysis, we will consider classic power-law path-loss and exp-law path-loss models. It is important to note that the analytical results we obtain for the distributions of $\widehat{s}_{pro}(\boldsymbol{X}^*_\times)$ and $\widehat{s}_{sum}(\boldsymbol{X}^*_+)$ can be used to obtain the performance metrics for general path-loss models obeying the product-scaling and sum-scaling property.

A. Distance Distribution for Optimum RIS Selection

For the sake of simplicity, we define $\Upsilon_{opt} \triangleq \widehat{s}_{pro}(\boldsymbol{X}^*_\times)$ and $\Lambda_{opt} \triangleq \widehat{s}_{sum}(\boldsymbol{X}^*_+)$. We now derive the distribution functions for Υ_{opt} and Λ_{opt} which are key to characterize the performance of the RIS selection policies $\mathcal{P}^*_{pro}$ and $\mathcal{P}^*_{sum}$, respectively. We will consider $\boldsymbol{x}_s = (-d, 0)^\top$ and $\boldsymbol{x}_d = (d, 0)^\top$ without loss of generality due to the stationary nature of HPPPs [37]. In the following theorems, we provide the distribution of Υ_{opt} and Λ_{opt}. We also numerically verify these distribution in Fig. 2.

Theorem 1: The CDF of Υ_{opt} is given by

$$F_{\Upsilon_{opt}}(\gamma) = \begin{cases} 1 - \exp\left(\frac{-2\lambda}{d^2}\left(d^4 E(\frac{\gamma^2}{d^4}) + (\gamma^2 - d^4)K(\frac{\gamma^2}{d^4})\right)\right) & \text{if } \gamma < d^2 \\ 1 - \exp\left(-2\lambda\gamma E(\frac{d^4}{\gamma^2})\right) & \text{if } \gamma \geq d^2 \end{cases}, \tag{8}$$

where $E(\cdot)$ is the complete elliptic integral of the second kind and $K(\cdot)$ is the complete elliptic integral of the first kind [38]. The PDF of Υ_{opt} is given by

$$f_{\Upsilon_{opt}}(\gamma) = \begin{cases} \frac{2}{d^2\gamma\lambda}\exp\left(-\frac{2\lambda}{d^2}\left(d^4 E\left(\frac{\gamma^2}{d^4}\right) + (\gamma^2 - d^4)K\left(\frac{\gamma^2}{d^4}\right)\right)\right)K\left(\frac{\gamma^2}{d^4}\right) & \text{if } \gamma < d^2 \\ 2\lambda\exp\left(-2\gamma\lambda E\left(\frac{d^4}{\gamma^2}\right)\right)K\left(\frac{d^4}{\gamma^2}\right) & \text{if } \gamma \geq d^2 \end{cases}. \tag{9}$$
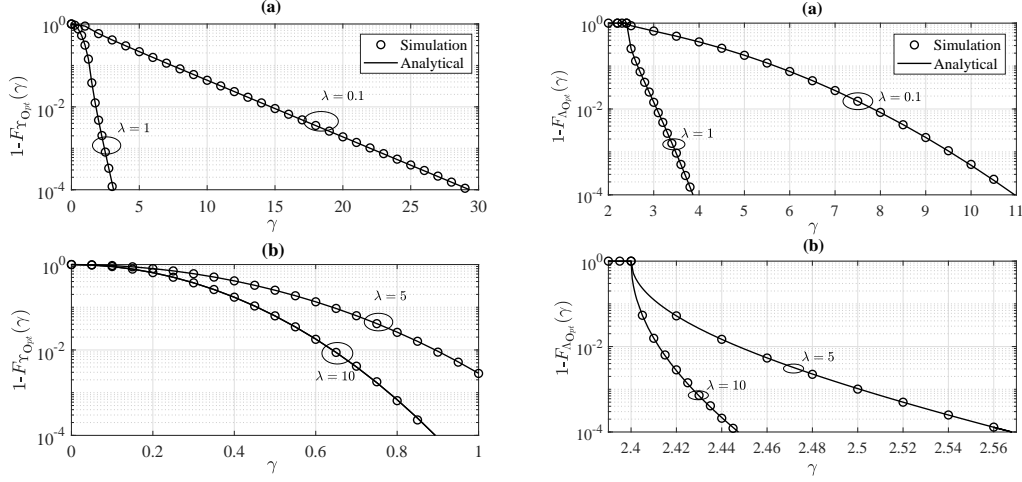
Fig. 2: The complementary CDF of Υ_{opt} and Λ_{opt} for different RIS densities $\lambda = 0.1, 1, 5, 10$ when $d = 1.2$, for validating (8) and (10), respectively.

Proof: See Appendix A. ∎

Theorem 2: The CDF of Λ_{opt} is given by

$$
F_{\Lambda_{\text{opt}}}(\gamma) = \begin{cases} 0 & \gamma < 2d \\ 1 - \exp\left(-\frac{\lambda\pi\gamma\sqrt{\gamma^2-4d^2}}{4}\right) & \gamma \geq 2d \end{cases}. \tag{10}
$$

The PDF of Λ_{opt} is given by

$$
f_{\Lambda_{\text{opt}}}(\gamma) = \begin{cases} 0 & \gamma < 2d \\ \frac{\pi\lambda\left(\gamma^2-2d^2\right)}{2\sqrt{\gamma^2-4d^2}}\exp\left(-\frac{\lambda\pi\gamma\sqrt{\gamma^2-4d^2}}{4}\right) & \gamma \geq 2d \end{cases}. \tag{11}
$$

Proof: See Appendix B. ∎

B. Averaged Performance Metrics over Fading Channel

Based on (6) and (7), we recall that $\mathsf{P}_{\text{out}}\left(\mathcal{P}\right)$ and $\mathsf{R}_{\text{ave}}\left(\mathcal{P}\right)$ relate to $\mathsf{SNR}\left(\mathcal{P},\Phi\right)$ and $\mathsf{R}\left(\mathcal{P},\Phi\right)$, respectively. To facilitate the derivation of P_{out} and R_{ave} for the optimum RIS selection policies $\mathcal{P}_{\text{pro}}^*$ and $\mathcal{P}_{\text{sum}}^*$, we derive $\mathsf{SNR}\left(\mathcal{P},\Phi\right)$ and $\mathsf{R}\left(\mathcal{P},\Phi\right)$ in this subsection. We derive $\mathsf{SNR}\left(\mathcal{P},\Phi\right)$ as

$$
\mathsf{SNR}\left(\mathcal{P},\Phi\right) = \mathsf{E}_Z\left[\frac{\bar{\gamma}Z^2}{G(\|\boldsymbol{x}_{\text{s}}-\boldsymbol{X}_{\mathcal{P}}\|,\|\boldsymbol{X}_{\mathcal{P}}-\boldsymbol{x}_{\text{d}}\|)}\right] = \frac{\bar{\gamma}\mathsf{E}_Z\left[Z^2\right]}{G(\|\boldsymbol{x}_{\text{s}}-\boldsymbol{X}_{\mathcal{P}}\|,\|\boldsymbol{X}_{\mathcal{P}}-\boldsymbol{x}_{\text{d}}\|)}, \tag{12}
$$

where $\mathsf{E}_Z\left[Z^2\right]$ is given by

$$
\mathsf{E}_Z\left[Z^2\right] = N + N(N-1)\frac{\pi^2}{16}. \tag{13}
$$

Applying (13) to (12), we have

$$
\mathsf{SNR}\left(\mathcal{P},\Phi\right) = \frac{\bar{\gamma}N(16+(N-1)\pi^2)}{16G(\|\boldsymbol{x}_{\text{s}}-\boldsymbol{X}_{\mathcal{P}}\|,\|\boldsymbol{X}_{\mathcal{P}}-\boldsymbol{x}_{\text{d}}\|)}. \tag{14}
$$

We next derive $\mathsf{R}\left(\mathcal{P}, \Phi\right)$ as

$$\mathsf{R}\left(\mathcal{P}, \Phi\right) = \mathsf{R}\left(\mathcal{P}, Y\right) = \mathsf{E}_Z\left[\log_2\left(1 + \bar{\gamma}Y Z^2\right)\right] = \int_0^\infty \log_2\left(1 + \bar{\gamma}Y z^2\right) f_Z(z)dz, \tag{15}$$

where $Y = \frac{1}{G(\|\boldsymbol{x}_\mathrm{s} - \boldsymbol{X}_\mathcal{P}\|, \|\boldsymbol{X}_\mathcal{P} - \boldsymbol{x}_\mathrm{d}\|)}$ and Y is a statistic summarising the overall effect of the point process Φ on the data rate. Based on (15), we study the distribution of Z. Since Z is a sum of the product of two i.i.d. Rayleigh RVs, its exact distribution is difficult to determine for $N > 1$. However, we can still approximate its distribution by using a gamma distribution with the shape parameter given by $k = \frac{N\pi^2}{16 - \pi^2}$ and the scale parameter given by $\theta = \frac{16 - \pi^2}{4\pi}$ very tightly, as established in [29], [33]. Using suggested gamma distribution approximation and the result in [33, Eq. (20)], we can express (15) as

$$\mathsf{R}\left(\mathcal{P}, Y\right) = \int_0^\infty \log_2\left(1 + \bar{\gamma}Y z^2\right) f_Z(z)dz \doteq \int_0^\infty \log_2\left(1 + \bar{\gamma}Y z^2\right) \frac{z^{k-1}\exp\left(-\frac{z}{\theta}\right)}{\theta^k \Gamma(k)}dz$$

$$\doteq \frac{1}{\log(2)}\left[2\log(\theta) + \log(\bar{\gamma}Y) + 2\psi^{(0)}(k) + \frac{{}_2\mathsf{F}_3\left(1, 1; 2, \frac{3}{2} - \frac{k}{2}, 2 - \frac{k}{2}; -\frac{1}{4\theta^2\bar{\gamma}Y}\right)}{\theta^2\bar{\gamma}Y\left(k^2 - 3k + 2\right)}\right.$$

$$\left. + \frac{\pi(\bar{\gamma}Y)^{-\frac{k}{2}}}{\theta^k\Gamma(k+1)}\left(\frac{{}_1\mathsf{F}_2\left(\frac{k}{2}; \frac{1}{2}, \frac{k}{2} + 1; -\frac{1}{4\theta^2\bar{\gamma}Y}\right)}{\left(\csc\left(\frac{\pi k}{2}\right)\right)^{-1}} - \frac{{}_1\mathsf{F}_2\left(\frac{k}{2} + \frac{1}{2}; \frac{3}{2}, \frac{k}{2} + \frac{3}{2}; -\frac{1}{4\theta^2\bar{\gamma}Y}\right)}{\sqrt{\bar{\gamma}Y}\theta(1+k)\left(k\sec\left(\frac{\pi k}{2}\right)\right)^{-1}}\right)\right] \tag{16}$$

where we use $\doteq$ to indicate that the equality is valid when the gamma approximation is applied, $\log(\cdot)$ denotes natural logarithm, ${}_p\mathsf{F}_q\left(\cdot; \cdot; \cdot\right)$ denotes the generalized hypergeometric functions [39], and $\psi^{(n)}(z)$ denotes the nth derivative of the digamma function [39]. Numerical results in Section V will confirm the accuracy of this approximation used in (16).

We note that the calculation of (16) requires high computational complexity. To ease the complexity, using Jensen's inequality, we can also derive an upper bound on $\mathsf{R}\left(\mathcal{P}, \Phi\right)$ as

$$\mathsf{R}\left(\mathcal{P}, \Phi\right) = \mathsf{E}_Z\left[\log_2\left(1 + \mathsf{SNR}_\mathrm{inst}\left(\mathcal{P}, \Phi, Z\right)\right)\right] \leq \log_2\left(1 + \mathsf{E}_Z\left[\mathsf{SNR}_\mathrm{inst}\left(\mathcal{P}, \Phi, Z\right)\right]\right). \tag{17}$$

By applying (14) to (17), we rewrite (17) as

$$\mathsf{R}\left(\mathcal{P}, Y\right) \leq \log_2\left(1 + \frac{\bar{\gamma}NY\left(16 + (N-1)\pi^2\right)}{16}\right), \tag{18}$$

where we write $\tilde{\mathsf{R}}\left(\mathcal{P}, Y\right) = \log_2\left(1 + \frac{\bar{\gamma}NY(16 + (N-1)\pi^2)}{16}\right)$ in the rest of the paper. We will use $\tilde{\mathsf{R}}\left(\mathcal{P}, Y\right)$ to calculate the upper bounds on the average rate in Section III-C2.

C. Performance Analysis

Based on subsections III-A and III-B, we evaluate the outage probability and average rate achieved by the optimum RIS selection policies $\mathcal{P}^*_\mathrm{pro}$ and $\mathcal{P}^*_\mathrm{sum}$. To illustrate specific applications of our results,

we will consider classical power-law and exp-law path-loss models for the performance evaluation in this subsection.

1) Outage Probability: We denote $\mathsf{P}_{\text{out}}^{\text{pow}}\left(\mathcal{P}_{\text{pro}}^{*}\right)$ and $\mathsf{P}_{\text{out}}^{\text{exp}}(\mathcal{P}_{\text{sum}}^{*})$ as the outage probabilities achieved under the power-law and exp-law path-loss models by the optimum RIS selection policies, respectively. Using (6) and applying[10] $G^{\text{pow}}(\|\boldsymbol{x}_{\text{s}} - \boldsymbol{X}_{\mathcal{P}}\|, \|\boldsymbol{X}_{\mathcal{P}} - \boldsymbol{x}_{\text{d}}\|) = (\|\boldsymbol{x}_{\text{s}} - \boldsymbol{X}_{\mathcal{P}}\| \|\boldsymbol{X}_{\mathcal{P}} - \boldsymbol{x}_{\text{d}}\|)^{\eta}$ to (14), we derive $\mathsf{P}_{\text{out}}^{\text{pow}}\left(\mathcal{P}_{\text{pro}}^{*}\right)$ as

$$
\begin{aligned}
\mathsf{P}_{\text{out}}^{\text{pow}}\left(\mathcal{P}_{\text{pro}}^{*}\right) &= \mathsf{Pr}\left\{\mathsf{SNR}\left(\mathcal{P}_{\text{pro}}^{*}, \Phi\right) \leq \rho\right\} = \mathsf{Pr}\left\{\frac{\bar{\gamma}N(16 + (N-1)\pi^2)}{16\Upsilon_{\text{opt}}^{\eta}} \leq \rho\right\} \\
&= 1 - F_{\Upsilon_{\text{opt}}}\left(\left(\frac{\bar{\gamma}N(16 + (N-1)\pi^2)}{16\rho}\right)^{\frac{1}{\eta}}\right),
\end{aligned}
\tag{19}
$$

where $F_{\Upsilon_{\text{opt}}}\left(\gamma\right)$ is the CDF of RV Υ_{opt} given in (8). Applying $G^{\text{exp}}(\|\boldsymbol{x}_{\text{s}} - \boldsymbol{X}_{\mathcal{P}}\|, \|\boldsymbol{X}_{\mathcal{P}} - \boldsymbol{x}_{\text{d}}\|) = \exp\left(\alpha\left(\|\boldsymbol{x}_{\text{s}} - \boldsymbol{X}_{\mathcal{P}}\| + \|\boldsymbol{X}_{\mathcal{P}} - \boldsymbol{x}_{\text{d}}\|\right)\right)$ to (14), we derive $\mathsf{P}_{\text{out}}^{\text{exp}}(\mathcal{P}_{\text{sum}}^{*})$ as

$$
\begin{aligned}
\mathsf{P}_{\text{out}}^{\text{exp}}(\mathcal{P}_{\text{sum}}^{*}) &= \mathsf{Pr}\left\{\mathsf{SNR}\left(\mathcal{P}_{\text{sum}}^{*}, \Phi\right) \leq \rho\right\} = \mathsf{Pr}\left\{\frac{\bar{\gamma}N(16 + (N-1)\pi^2)}{16\exp\left(\alpha\Lambda_{\text{opt}}\right)} \leq \rho\right\} \\
&= \mathsf{Pr}\left\{\Lambda_{\text{opt}} > \log\left(\frac{\bar{\gamma}N(16 + (N-1)\pi^2)}{16\rho}\right)\alpha^{-1}\right\} \\
&= 1 - F_{\Lambda_{\text{opt}}}\left(\frac{1}{\alpha}\log\left(\frac{\bar{\gamma}N(16 + (N-1)\pi^2)}{16\rho}\right)\right).
\end{aligned}
\tag{20}
$$

where $F_{\Lambda_{\text{opt}}}\left(\gamma\right)$ is the CDF of RV Λ_{opt} given in (10).

2) Average Rate: We denote $\mathsf{R}_{\text{ave}}^{\text{pow}}\left(\mathcal{P}_{\text{pro}}^{*}\right)$ and $\mathsf{R}_{\text{ave}}^{\text{exp}}\left(\mathcal{P}_{\text{sum}}^{*}\right)$ as the data rate obtained under the power-law and exp-law path-loss models by the optimum RIS selection policies, respectively. Based on the definition of $\mathsf{R}_{\text{ave}}\left(\mathcal{P}\right)$ in (7), we evaluate $\mathsf{R}_{\text{ave}}^{\text{pow}}\left(\mathcal{P}_{\text{pro}}^{*}\right)$ as

$$
\mathsf{R}_{\text{ave}}^{\text{pow}}\left(\mathcal{P}_{\text{pro}}^{*}\right) = \mathsf{E}_{\Phi}\left[\mathsf{R}\left(\mathcal{P}, Y_{\text{pow}}\right)\right] = \int \mathsf{R}\left(\mathcal{P}, y\right) f_{Y_{\text{pow}}}(y) d y,
\tag{21}
$$

where y is a realization of RV Y_{pow} and $Y_{\text{pow}} = \frac{1}{G^{\text{pow}}(\|\boldsymbol{x}_{\text{s}} - \boldsymbol{X}_{\times}^{*}\|, \|\boldsymbol{X}_{\times}^{*} - \boldsymbol{x}_{\text{d}}\|)} = \Upsilon_{\text{opt}}^{-\eta}$. We note that $\mathsf{R}\left(\mathcal{P}, Y_{\text{pow}}\right)$ is given by (16). Using the distribution of Υ_{opt}, we derive the PDF of $Y_{\text{pow}} = \Upsilon_{\text{opt}}^{-\eta}$ as

$$
f_{Y_{\text{pow}}}\left(y\right) = \begin{cases} S_1\left(y\right) = \dfrac{2\exp\left(-2y^{-\frac{1}{\eta}}\lambda E(d^4 y^{\frac{2}{\eta}})\right)y^{-1-\frac{1}{\eta}}\lambda K(d^4 y^{\frac{2}{\eta}})}{} & \text{if } 0 < y \leq d^{-2\eta} \\[4ex] S_2\left(y\right) = \dfrac{2\exp\left(-\dfrac{2\lambda\left(d^4 E\left(\dfrac{y^{\frac{-2}{\eta}}}{d^4}\right) + \left(-d^4 + y^{\frac{-2}{\eta}}\right)K\left(\dfrac{y^{\frac{-2}{\eta}}}{d^4}\right)\right)}{d^2}\right)y^{\frac{-2+\eta}{\eta}}\lambda K\left(\dfrac{y^{\frac{-2}{\eta}}}{d^4}\right)}{d^2\eta} & \text{if } y \geq d^{-2\eta} \end{cases}.
\tag{22}
$$

---

[10]We assume that the path-loss exponents of the TX-RIS and RIS-RX channels are the same. This assumption is reasonable when the TX-RIS and RIS-RX channels have similar propagation environments.

There is no closed form expression for $\mathsf{R}_{\mathrm{ave}}^{\mathrm{pow}}\left(\mathcal{P}_{\mathrm{pro}}^{*}\right)$ but it can be evaluated numerically with the aid of (16), (21), and (22) by calculating the integrals given below:

$$\mathsf{R}_{\mathrm{ave}}^{\mathrm{pow}}\left(\mathcal{P}_{\mathrm{pro}}^{*}\right) = \int_{0}^{d^{-2\eta}} \mathsf{R}\left(\mathcal{P}, y\right) S_{1}\left(y\right) d\,y + \int_{d^{-2\eta}}^{\infty} \mathsf{R}\left(\mathcal{P}, y\right) S_{2}\left(y\right) d\,y. \tag{23}$$

As (21), we write $\mathsf{R}_{\mathrm{ave}}^{\mathrm{exp}}\left(\mathcal{P}_{\mathrm{sum}}^{*}\right)$ as

$$\mathsf{R}_{\mathrm{ave}}^{\mathrm{exp}}\left(\mathcal{P}_{\mathrm{sum}}^{*}\right) = \int \mathsf{R}\left(\mathcal{P}, y\right) f_{Y_{\mathrm{exp}}}(y) d\,y, \tag{24}$$

where y is a realization of Y_{exp} and $Y_{\mathrm{exp}} = \exp\left(-\alpha \Lambda_{\mathrm{opt}}\right)$. $\mathsf{R}\left(\mathcal{P}, Y_{\mathrm{exp}}\right)$ is given by (16). We then derive the PDF of Y_{exp}. By using variable transformation and $f_{\Lambda_{\mathrm{opt}}}\left(\gamma\right)$ in (11), the PDF of Y_{exp} can be derived as

$$f_{Y_{\mathrm{exp}}}(y) = \frac{\pi y^{\frac{\pi\lambda\sqrt{\frac{\log^{2}\left(\frac{1}{y}\right)}{\alpha^{2}} - 4d^{2}}}{4\alpha} - 1}\lambda\left(\frac{\log^{2}\left(\frac{1}{y}\right)}{\alpha^{2}} - 2d^{2}\right)}{2\alpha\sqrt{\frac{\log^{2}\left(\frac{1}{y}\right)}{\alpha^{2}} - 4d^{2}}}, \tag{25}$$

for $y \leq e^{-2\alpha d}$. $f_{Y_{\mathrm{exp}}}(y)$ is zero for $y > e^{-2\alpha d}$. With the aid of (16), (24) and (25), the average rate can be numerically calculated by evaluating the integral

$$\mathsf{R}_{\mathrm{ave}}^{\mathrm{exp}}\left(\mathcal{P}_{\mathrm{sum}}^{*}\right) = \int_{0}^{e^{-2\alpha d}} \mathsf{R}\left(\mathcal{P}, y\right) f_{Y_{\mathrm{exp}}}(y) d\,y. \tag{26}$$

Remark 1: The upper bounds on $\mathsf{R}_{\mathrm{ave}}^{\mathrm{pow}}\left(\mathcal{P}_{\mathrm{pro}}^{*}\right)$ and $\mathsf{R}_{\mathrm{ave}}^{\mathrm{exp}}\left(\mathcal{P}_{\mathrm{sum}}^{*}\right)$ via Jensen's inequality can be obtained by replacing $\mathsf{R}\left(\mathcal{P}, y\right)$ by $\tilde{\mathsf{R}}\left(\mathcal{P}, y\right)$ in (23) and (26), where $\tilde{\mathsf{R}}\left(\mathcal{P}, Y\right)$ is given in (18).

IV. LIMITED-FEEDBACK RIS SELECTION

In previous sections, we consider that there exists a central entity (i.e., a network controller) knowing the locations of all RISs to perform the selection based on this knowledge by optimising either product or sum distances without feedback. Different from previous sections, in this section, we assume the existence of extra feedback capability at RISs for distributed operation. We assume that the RISs can feed back their channel quality indicators[11], *whilst* still functioning as the nearly passive elements for communications after the feedback phase.

In this section, we propose a limited-feedback RIS selection policy that selects the best RIS from a limited number of RISs feeding back. We will first derive the distribution of the number of RISs feeding back under the product-scaling and sum-scaling path-loss models. We will then evaluate the

---

[11]An RIS can know its channel quality by employing some active sensors among the passive reflective elements at the RISs as proposed in [40] or deploying anchor nodes near the RISs as proposed in [41].
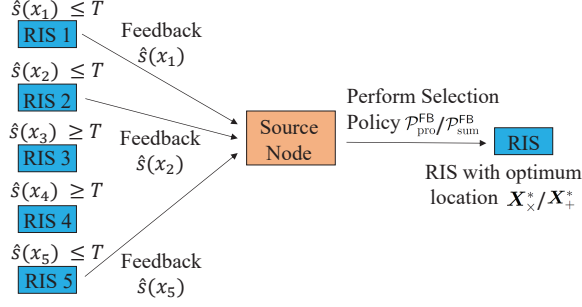
Fig. 3: An example illustration for the limited-feedback RIS selection with 5 potential RISs. RIS1, RIS2, and RIS5, whose the channel quality indicators $\widehat{s}(\boldsymbol{x}_1)$, $\widehat{s}(\boldsymbol{x}_2)$, $\widehat{s}(\boldsymbol{x}_5)$ are less than the given threshold value T, send their channel quality indicators to the source node. The source node then performs selection policy $\mathcal{P}_{\mathrm{pro}}^{\mathsf{FB}}$ or $\mathcal{P}_{\mathrm{sum}}^{\mathsf{FB}}$ to select the RIS with optimum location $\boldsymbol{X}_{\times}^{*}$ or $\boldsymbol{X}_{+}^{*}$.

average rate and outage probability attained by the proposed limited-feedback RIS selection policy under the specific path-loss models. To illustrate specific applications of our results, we will consider classic power-law and exp-law path-loss models for the performance evaluation in this section. We note that the derivation method used to obtain the performance metrics under power-law and exp-law path-loss models can be also used for other path-loss models.

A. Limited-Feedback Strategy

To alleviate the feedback overhead, we will consider an effective yet simple limited-feedback strategy (illustrated in Fig. 3), which is formally put forward as follows.

Limited-Feedback Strategy: An RIS located at $\boldsymbol{X} \in \Phi$ will send its channel quality indicator $\widehat{s}(\boldsymbol{X})$ back to the source node when $\widehat{s}(\boldsymbol{X}) \leq T$, where $T > 0$ is a given threshold value. For the product-scaling path-loss law, $\widehat{s}(\boldsymbol{X})$ is $\widehat{s}(\boldsymbol{X}) = \widehat{s}_{\mathrm{pro}}(\boldsymbol{X})$, where $\widehat{s}_{\mathrm{pro}}(\boldsymbol{X})$ is given by $\widehat{s}_{\mathrm{pro}}(\boldsymbol{X}) = \|\boldsymbol{x}_{\mathrm{s}} - \boldsymbol{X}\| \times \|\boldsymbol{X} - \boldsymbol{x}_{\mathrm{d}}\|$. For the sum-scaling path-loss law, $\widehat{s}(\boldsymbol{X})$ is $\widehat{s}(\boldsymbol{X}) = \widehat{s}_{\mathrm{sum}}(\boldsymbol{X})$, where $\widehat{s}_{\mathrm{sum}}(\boldsymbol{X})$ is $\widehat{s}_{\mathrm{sum}}(\boldsymbol{X}) = \|\boldsymbol{x}_{\mathrm{s}} - \boldsymbol{X}\| + \|\boldsymbol{X} - \boldsymbol{x}_{\mathrm{d}}\|$. If no RIS feeds back its channel quality indicator, no data is transmitted by the source node.

We will characterize the number of RISs feeding back given the aforementioned feedback strategy and evaluate the average rate and outage probability attained by limited-feedback RIS selection policies in the following subsections.

B. Distribution of the Feedback Load with Limited-Feedback

Given the feedback strategy proposed in subsection IV-A, we denote the total number of RISs feeding back under the product-scaling and the sum-scaling RIS selection function by $N_{\mathrm{pro}}^{\mathsf{FB}}$ and $N_{\mathrm{sum}}^{\mathsf{FB}}$,

respectively. That is, $N_{\text{pro}}^{\text{FB}} = \sum_{\boldsymbol{X} \in \Phi} 1_{\{\widehat{s}_{\text{pro}}(\boldsymbol{X}) \leq T_{\text{pro}}\}}$ and $N_{\text{sum}}^{\text{FB}} = \sum_{\boldsymbol{X} \in \Phi} 1_{\{\widehat{s}_{\text{sum}}(\boldsymbol{X}) \leq T_{\text{sum}}\}}$, where $1_{\{\cdot\}}$ is the indicator function. T_{pro} and T_{sum} are the thresholds used in the product-scaling and sum-scaling scenarios, respectively. The average number of RISs feeding back is given by $\Xi_{\text{pro}} = \mathsf{E}_{\Phi}\left[N_{\text{pro}}^{\text{FB}}\right]$ and $\Xi_{\text{sum}} = \mathsf{E}_{\Phi}\left[N_{\text{sum}}^{\text{FB}}\right]$. The sets of the RISs feeding back are given by $\Phi_{\text{pro}}^{\text{FB}} = \{X \in \Phi : \widehat{s}_{\text{pro}}(\boldsymbol{X}) \leq T_{\text{pro}}\}$ and $\Phi_{\text{sum}}^{\text{FB}} = \{X \in \Phi : \widehat{s}_{\text{sum}}(\boldsymbol{X}) \leq T_{\text{sum}}\}$.

We now formulate the RIS selection policy with limited-feedback for the power-law and exp-law path-loss models as follows:

Selection Policy 3: The RIS selection policy with limited-feedback strategy under the product-scaling path-loss law, denoted by $\mathcal{P}_{\text{pro}}^{\text{FB}}$, is the one that solves the following optimization problem

$$\begin{aligned} \underset{\boldsymbol{X} \in \mathbb{R}^2}{\text{minimize}} \quad & \widehat{s}_{\text{pro}}(\boldsymbol{X}) \\ \text{subject to} \quad & \boldsymbol{X} \in \Phi_{\text{pro}}^{\text{FB}} \end{aligned}. \tag{27}$$

Selection Policy 4: For the sum-scaling path-loss law, the RIS selection policy with limited-feedback strategy, denoted by $\mathcal{P}_{\text{sum}}^{\text{FB}}$, is the one that solves the following optimization problem

$$\begin{aligned} \underset{\boldsymbol{X} \in \mathbb{R}^2}{\text{minimize}} \quad & \widehat{s}_{\text{sum}}(\boldsymbol{X}) \\ \text{subject to} \quad & \boldsymbol{X} \in \Phi_{\text{sum}}^{\text{FB}} \end{aligned}. \tag{28}$$

Derivation of the distributions of $N_{\text{pro}}^{\text{FB}}$ and $N_{\text{sum}}^{\text{FB}}$ is a key step to quantify the performance attained by $\mathcal{P}_{\text{pro}}^{\text{FB}}$ and $\mathcal{P}_{\text{sum}}^{\text{FB}}$. We present the distributions of $N_{\text{pro}}^{\text{FB}}$ and $N_{\text{sum}}^{\text{FB}}$ in the following theorems.

Theorem 3: $N_{\text{pro}}^{\text{FB}}$ is a Poisson RV with the mean Ξ_{pro} given by

$$\Xi_{\text{pro}} = \begin{cases} 2\lambda \left(\frac{1}{d^2} \left(d^4 E(\frac{T_{\text{pro}}^2}{d^4}) + (T_{\text{pro}}^2 - d^4) K(\frac{T_{\text{pro}}^2}{d^4}) \right) \right) & \text{if } T_{\text{pro}} \leq d^2 \\ 2\lambda \left(T_{\text{pro}} E(\frac{d^4}{T_{\text{pro}}^2}) \right) & \text{if } T_{\text{pro}} > d^2 \end{cases}. \tag{29}$$

Proof: See Appendix C. ∎

Theorem 4: $N_{\text{sum}}^{\text{FB}}$ is a Poisson RV with the mean Ξ_{sum} given by

$$\Xi_{\text{sum}} = \begin{cases} 0 & \text{if } T_{\text{sum}} \leq 2d \\ \frac{\lambda \pi T_{\text{sum}}}{4} \sqrt{-4d^2 + T_{\text{sum}}^2} & \text{if } T_{\text{sum}} > 2d \end{cases}. \tag{30}$$

Proof: The proof is similar to the one given for Theorem 3. Hence, it is omitted to avoid repetitions. ∎

In Fig. 4, we plot the expected numbers of RISs feeding back and compare the simulated distribution of the total number of RISs feeding back with the Poisson distribution with analytical means in (29) and (30). We observe that simulated distributions match the theoretical ones perfectly, which validates the Theorems 3 and 4. As discussed in [28], the threshold value $\Xi_{\text{pro}} \geq 5$ enables the limited-feedback RIS selection strategy to achieve very similar outage and data rate performance as the centralized
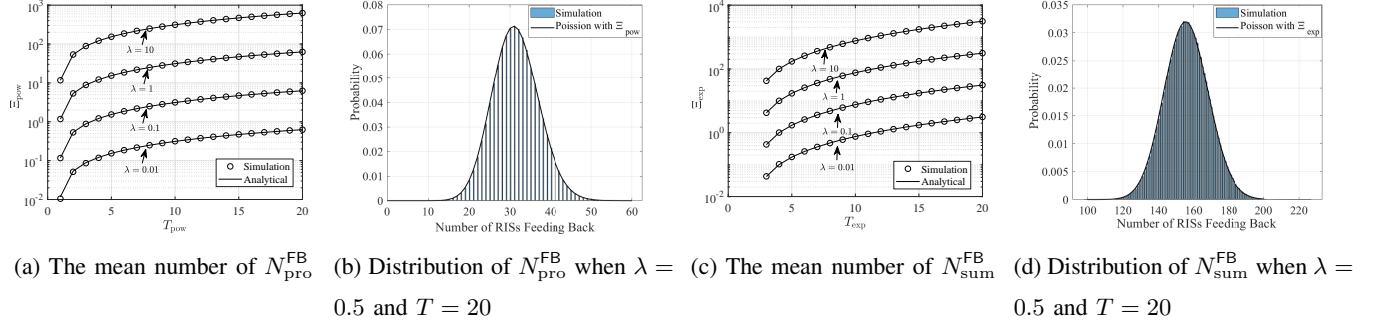
(a) The mean number of $N_{\mathrm{pro}}^{\mathsf{FB}}$ (b) Distribution of $N_{\mathrm{pro}}^{\mathsf{FB}}$ when $\lambda =$ (c) The mean number of $N_{\mathrm{sum}}^{\mathsf{FB}}$ (d) Distribution of $N_{\mathrm{sum}}^{\mathsf{FB}}$ when $\lambda =$
0.5 and $T = 20$ 0.5 and $T = 20$

Fig. 4: Average number of RISs feeding back and probability distribution of the number of RISs feeding back for $d = 1.2$ for product-scaling path-loss law in Figs. 2(a) and 2(b) and for sum-scaling path-loss law in Figs. 2(c) and 2(d).

RIS selection strategy, while providing a massive reduction in the feedback overhead. This is because the RIS with optimum location, $\boldsymbol{X}_{\times}^{*}$, always feeds its channel quality indicators back to the source node if $N_{\mathrm{pro}}^{\mathsf{FB}} \geq 1$ and $\mathsf{Pr}\left\{N_{\mathrm{pro}}^{\mathsf{FB}} \geq 1\right\} \geq 0.99$ when $\Xi_{\mathrm{pro}} > 5$ due to the exponentially decaying tail of Poisson distribution. The same arguments also apply to the sum-scaling path loss models.

C. Performance Analysis

We next evaluate the outage probability and average rate attained by the limited-feedback RIS selection policies, parameterized by the threshold values T_{pro} and T_{sum}, for the power-law and exp-law path-loss models, respectively.

The outage probability with limited feedback for the power-law and exp-law path-loss models are given in the following theorems:

Theorem 5: The outage probability $\mathsf{P}_{\mathrm{out}}^{\mathrm{pow}}\left(\mathcal{P}_{\mathrm{pro}}^{\mathsf{FB}}\right)$ for a limited-feedback RIS selection policy $\mathcal{P}_{\mathrm{pro}}^{\mathsf{FB}}$ with threshold T_{pro} is equal to

$$\mathsf{P}_{\mathrm{out}}^{\mathrm{pow}}\left(\mathcal{P}_{\mathrm{pro}}^{\mathsf{FB}}\right) = \begin{cases} \exp\left(-\Xi_{\mathrm{pro}}\right) & \text{if } \rho \leq \frac{\bar{\gamma}N(16+(N-1)\pi^2)}{T_{\mathrm{pro}}^{\eta}16} \\ 1 - F_{\Upsilon_{\mathrm{opt}}}\left(\left(\frac{\bar{\gamma}N(16+(N-1)\pi^2)}{\rho 16}\right)^{\frac{1}{\eta}}\right) & \text{otherwise} \end{cases}, \quad (31)$$

where Ξ_{pro} is the average feedback load at T_{pro} and given in (29).

Proof: To prove Theorem 5, we first write the outage event as follows:

$$\left\{\mathsf{E}_Z\left[\mathsf{SNR}^{\mathrm{pow}}\left(\mathcal{P}_{\mathrm{pro}}^{*}\right)\right] \leq \rho\right\} = \left\{\Upsilon_{\mathrm{opt}} > T_{\mathrm{pro}}\right\} \bigcup \left(\left\{\Upsilon_{\mathrm{opt}} \leq T_{\mathrm{pro}}\right\} \bigcap \left\{\frac{\bar{\gamma}N(16+(N-1)\pi^2)}{\Upsilon_{\mathrm{opt}}^{\eta}16} \leq \rho\right\}\right).$$

Hence, $\mathsf{P}_{\mathrm{out}}\left(\mathcal{P}_{\mathrm{pro}}^{\mathsf{FB}}\right)$ is given by

$$\mathsf{P}_{\mathrm{out}}\left(\mathcal{P}_{\mathrm{pro}}^{\mathsf{FB}}\right) = \mathsf{Pr}\left\{\Upsilon_{\mathrm{opt}} > T_{\mathrm{pro}}\right\} + \mathsf{Pr}\left(\left\{\Upsilon_{\mathrm{opt}} \leq T_{\mathrm{pro}}\right\} \bigcap \left\{\frac{\bar{\gamma}N(16+(N-1)\pi^2)}{\Upsilon_{\mathrm{opt}}^{\eta}16} \leq \rho\right\}\right)$$

$$= \exp\left(-\Xi_{\mathrm{pro}}\right) + \mathsf{Pr}\left\{\frac{\bar{\gamma}N(16+(N-1)\pi^2)}{T_{\mathrm{pro}}^{\eta}16} \leq \frac{\bar{\gamma}N(16+(N-1)\pi^2)}{\Upsilon_{\mathrm{opt}}^{\eta}16} \leq \rho\right\}. \quad (32)$$

If $\rho < \frac{\bar{\gamma}N(16+(N-1)\pi^2)}{T_{\mathrm{pro}}^{\eta}16}$, then the second summand in (32) becomes zero, and we have

$\mathsf{P}_{\mathrm{out}}\left(\mathcal{P}_{\mathrm{FB}}, T_{\mathrm{pro}}\right) = \exp\left(-\Xi_{\mathrm{pro}}\right)$, which is the first condition in (31). If $\rho > \frac{\bar{\gamma}N(16+(N-1)\pi^2)}{T_{\mathrm{pro}}^{\eta}16}$, we have

$\mathsf{P}_{\mathrm{out}}\left(\mathcal{P}_{\mathrm{FB}}, T\right) = \mathsf{Pr}\left\{\frac{\bar{\gamma}N(16+(N-1)\pi^2)}{\Upsilon_{\mathrm{opt}}^{\eta}16} \leq \rho\right\} = 1 - F_{\Upsilon_{\mathrm{opt}}}\left(\left(\frac{\bar{\gamma}N(16+(N-1)\pi^2)}{\rho16}\right)^{\frac{1}{\eta}}\right)$, which is the second

condition in (31). This completes the proof of Theorem 5. ∎

Theorem 6: The outage probability $\mathsf{P}_{\mathrm{out}}^{\exp}\left(\mathcal{P}_{\mathrm{sum}}^{\mathsf{FB}}\right)$ for a limited-feedback RIS selection policy $\mathcal{P}_{\mathrm{pro}}^{\mathsf{FB}}$

with threshold T_{sum} is given by

$$\mathsf{P}_{\mathrm{out}}^{\exp}\left(\mathcal{P}_{\mathrm{sum}}^{\mathsf{FB}}\right) = \begin{cases} \exp\left(-\Xi_{\mathrm{sum}}\right) & \text{if } \rho \leq \frac{\bar{\gamma}N(16+(N-1)\pi^2)}{\exp(\alpha T_{\mathrm{sum}})16} \\ 1 - F_{\Lambda_{\mathrm{opt}}}\left(\log\left(\frac{\bar{\gamma}N(16+(N-1)\pi^2)}{\rho16}\right)\alpha^{-1}\right) & \text{if } \frac{\bar{\gamma}N(16+(N-1)\pi^2)}{\exp(\alpha T_{\mathrm{sum}})16} < \rho < \frac{\bar{\gamma}N(16+(N-1)\pi^2)}{\exp(\alpha 2d)16} \\ 1 & \text{if } \rho \geq \frac{\bar{\gamma}N(16+(N-1)\pi^2)}{\exp(\alpha 2d)16} \end{cases}.$$

(33)

Proof: Theorem 6 can be proven similarly to Theorem 5. ∎

We evaluate the average rate achieved by $\mathcal{P}_{\mathrm{pro}}^{\mathsf{FB}}$ and $\mathcal{P}_{\mathrm{sum}}^{\mathsf{FB}}$ in the following theorems:

Theorem 7: The average rate $\mathsf{R}_{\mathrm{ave}}^{\mathrm{pow}}\left(\mathcal{P}_{\mathrm{pro}}^{\mathsf{FB}}\right)$ for a limited-feedback RIS selection policy $\mathcal{P}_{\mathrm{pro}}^{\mathsf{FB}}$ with

threshold T_{pro} is given by

$$\mathsf{R}_{\mathrm{ave}}^{\mathrm{pow}}\left(\mathcal{P}_{\mathrm{pro}}^{\mathsf{FB}}\right) = \int_{T_{\mathrm{pro}}^{-\eta}}^{d^{-2\eta}} \mathsf{R}\left(\mathcal{P}, y\right) S_1\left(y\right) d\,y + \int_{d^{-2\eta}}^{\infty} \mathsf{R}\left(\mathcal{P}, y\right) S_2\left(y\right) d\,y.$$

(34)

Proof: Theorem 7 can be proven by using the equivalence of events $\left\{N_{\mathrm{pro}}^{\mathsf{FB}} \geq 1\right\}$ and $\left\{\Upsilon_{\mathrm{opt}} > T_{\mathrm{pro}}\right\}$.

∎

Theorem 8: The average rate $\mathsf{R}_{\mathrm{ave}}^{\exp}\left(\mathcal{P}_{\mathrm{sum}}^{\mathsf{FB}}\right)$ for a given limited-feedback RIS selection policy $\mathcal{P}_{\mathrm{sum}}^{\mathsf{FB}}$

with threshold T_{sum} is equal to

$$\mathsf{R}_{\mathrm{ave}}^{\exp}\left(\mathcal{P}_{\mathrm{sum}}^{\mathsf{FB}}\right) = \int_{\exp(-\alpha T_{\mathrm{sum}})}^{e^{-2\alpha d}} \mathsf{R}\left(\mathcal{P}, y\right) f_{Y_{\exp}}(y) d\,y.$$

(35)

Proof: Theorem 8 can be proven similarly to Theorem 7. ∎

We note that the upper bounds on $\mathsf{R}_{\mathrm{ave}}^{\mathrm{pow}}\left(\mathcal{P}_{\mathrm{pro}}^{\mathsf{FB}}\right)$ and $\mathsf{R}_{\mathrm{ave}}^{\exp}\left(\mathcal{P}_{\mathrm{sum}}^{\mathsf{FB}}\right)$ using Jensen's inequality can be

obtained as in Remark 1.

V. NUMERICAL RESULTS

In this section, we present simulation and numerical results to verify our derived analytical results,

discuss the performance of the proposed centralized and limited-feedback RIS selection policies, and

reveal the effect of system parameters on the system performance.

In our simulations, the target SNR and the distance between TX and RX are set to $\rho = 5\,\mathrm{dB}$ and

$d = 1.2\,\mathrm{m}$, respectively. The unit for λ is RISs/m^2 and the value of λ will be mentioned in each

figure. For the performance evaluation, the path-loss exponent η is taken to be 4 and the tunable
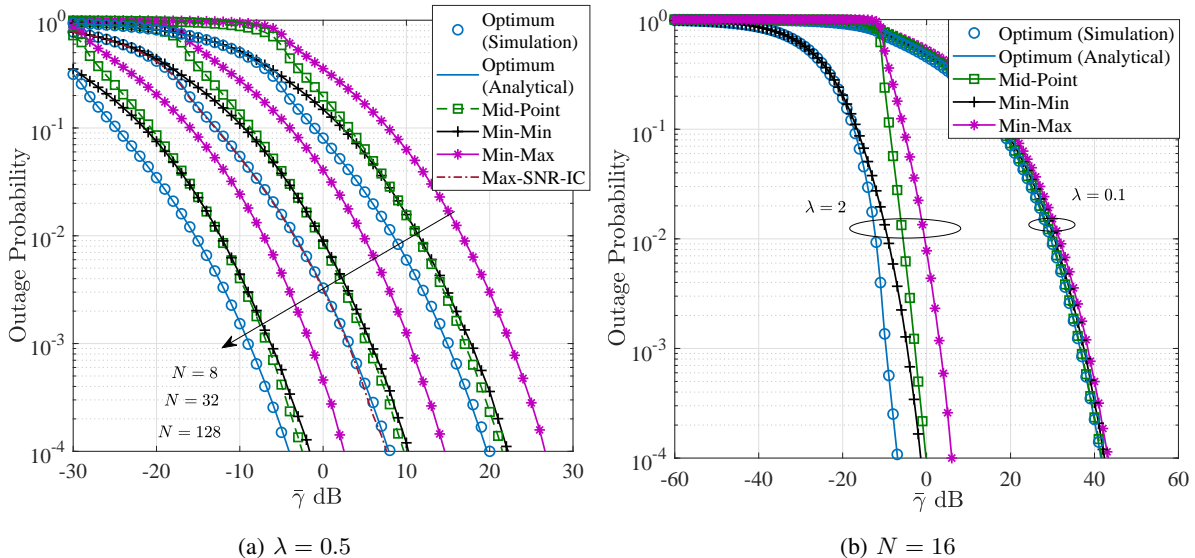
(a) $\lambda = 0.5$

(b) $N = 16$

Fig. 5: Outage probability achieved by different RIS selection schemes versus average SNR $\bar{\gamma}$, $d = 1.2$, $\eta = 4$, $\rho = 5$ dB, for the power-law path-loss model.

parameter α of the exp path-loss model is 1.037 [35]. The simulation results are averaged over many realizations of the random locations of RISs and channel fading.

A. Centralized RIS Selection

In this subsection, we focus on the performance of optimum centralized RIS selection policies. To benchmark the optimum selection policy, we consider three other RIS selection schemes:

1) *Min-min* scheme selects the closet RIS to the TX and RX set $\{\boldsymbol{x}_{\mathrm{s}}, \boldsymbol{x}_{\mathrm{d}}\}$, i.e.,

$$\underset{\boldsymbol{X} \in \mathbb{R}^2}{\text{minimize}} \ \min \left\{ \|\boldsymbol{x}_{\mathrm{s}} - \boldsymbol{X}\|, \|\boldsymbol{X} - \boldsymbol{x}_{\mathrm{d}}\| \right\}, \ \boldsymbol{X} \in \Phi;$$

2) *Min-max* scheme selects an RIS according to

$$\underset{\boldsymbol{X} \in \mathbb{R}^2}{\text{minimize}} \ \max \left\{ \|\boldsymbol{x}_{\mathrm{s}} - \boldsymbol{X}\|, \|\boldsymbol{X} - \boldsymbol{x}_{\mathrm{d}}\| \right\}, \ \boldsymbol{X} \in \Phi;$$

which is the optimum scheme for a decode-and-forward relay network [28];

3) *Mid-point* scheme selects the RIS that has the minimal distance to the mid-point between the TX and the RX.

In Figs. 5 and 6, we investigate the performance for power-law communications scenarios under the optimum and other different RIS selection schemes as described above. In Fig 5, we plot the outage probability curves versus the average SNR for $N = 8$, $N = 32$ and $N = 128$ (i.e., see Fig. 5a) and for $\lambda = 0.1$ and 2 (i.e., see Fig. 5b). In Fig. 5, analytical curves are obtained by using (19). The perfect agreement between analytical and simulation curves verifies the outage probability expression

for the optimum RIS selection scheme in (19). In Fig. 5a, we also plot max-SNR-instantaneous-channel (max-SNR-IC) scheme that selects the RIS yielding the largest instantaneous SNR based on the instantaneous channels. In Fig. 5a, we first see the outage probability decreases significantly when the number of elements increases from 8 to 32, where an RIS with $N = 8$ requires around 15 times more power than an RIS with $N = 32$ to achieve the outage probability level of 10^{-3}. For $N = 8, 32$ and 128, the optimum scheme has the best performance among all schemes. We see that max-SNR-IC slightly outperforms the optimum policy. We note that the max-SNR-IC scheme is actually the optimal RIS selection policy, but this scheme is more difficult to be implemented than the optimum scheme proposed in the paper since max-SNR-IC requires the knowledge of instantaneous fading channels of all available RIS-aided links. Among the other three schemes, min-min is the best suboptimal one when the average SNR $\bar{\gamma}$ is less than 0 dB; otherwise, mid-point is the best suboptimal one. For example, the optimum scheme only requires around 63% transmit power that mid-point scheme requires to achieve the outage probability level of 10^{-3}. Further, min-max always has the worst performance among these four schemes. In Fig. 5b, we observe a significant decrease in outage probability when the density increases from $\lambda = 0.1$ to $\lambda = 2$. When λ is very small as 0.1, all selection schemes have very similar performance. This observation indicates there is a high probability to select the same RIS by different schemes at a very low RIS density and the superiority of the optimum scheme is not obvious. However, the performance gap clearly increases with λ. For example, when λ is 2, the optimum scheme only requires around 32% transmit power that min-min scheme requires to achieve the outage probability level of 10^{-3}.

We plot the average rate versus $\bar{\gamma}$ in Fig. 6a and the average rate versus the density in Fig. 6b. We only consider the optimum scheme and min-min scheme since these two schemes generally outperform the other two schemes for different sets of parameters based on Fig 5. Analytical values calculated from (23) has a perfect agreement with the simulation, which verifies the accuracy of our analysis. In Fig. 6, we see that the optimum and min-min selection schemes have small rate differences for different values of N at $\lambda = 0.5$. For example, the rate difference is around 0.3 [bits/sec/Hz] for $N = 16$ at $\mathsf{SNR} = 5$ dB. Interestingly, the average rate increases almost linearly with SNR and the gap between the optimum scheme and min-min scheme keeps unchanged as the average SNR increases. In Fig. 6b, we see the average rate for both schemes increases as the RIS density increases, but the increase in average rate with the density is not linear as that with the average SNR. In addition, we observe that the upper bounds obtained via Jensen's inequality is tighter as N increases. Similar observations will be illustrated in Fig. 8 as well.
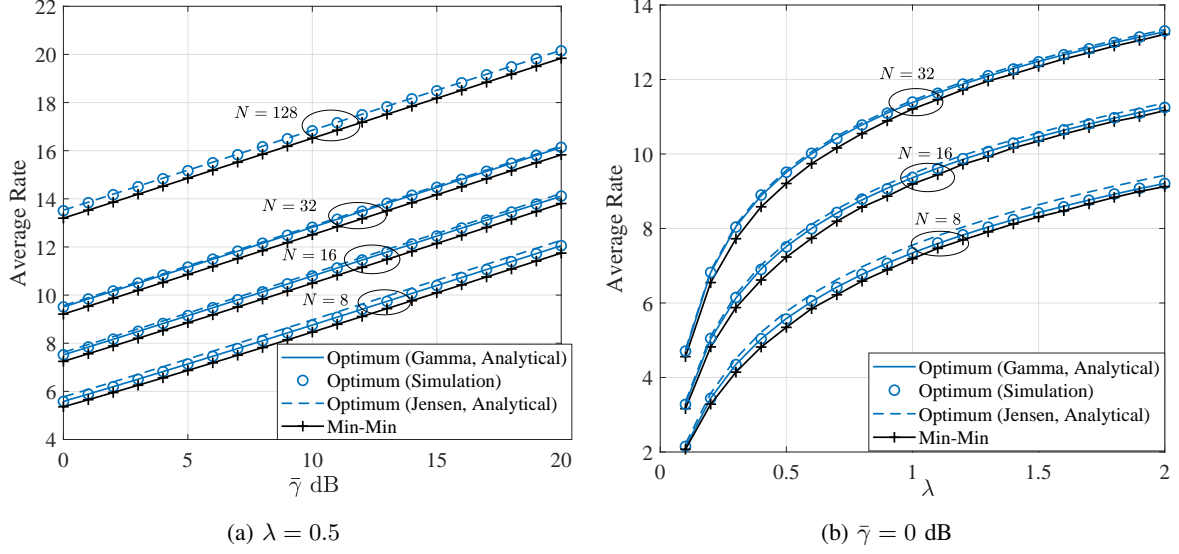
Fig. 6: Average rate achieved by different RIS selection schemes for different values of N, $d = 1.2$, $\eta = 4$, for the power-law path-loss model.
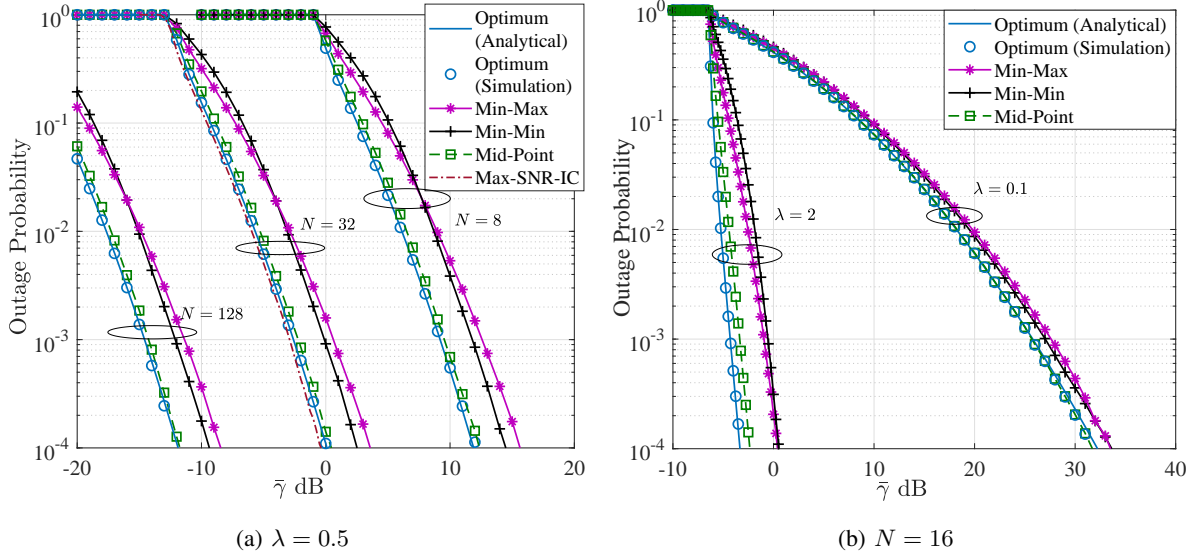

Fig. 7: Outage probability achieved by different RIS selection schemes versus average SNR $\bar{\gamma}$, $d = 1.2$, $\alpha = 1.037$, $\rho = 5$ dB, for the exp-law path-loss model.

In Figs. 7 and 8, we focus on the performance of the exp-law path-loss model. In Fig. 7, we plot the outage probability curves versus SNR for $N = 8$, $N = 32$ and $N = 128$ (i.e., see Fig. 7a) and for $\lambda = 0.1$ and 2 (i.e., see Fig. 7b). Analytical curves obtained by (20) match with the simulations, thus validating the accuracy of (20). The optimum and max-SNR-IC schemes outperform the other schemes, which is similar to the observations in Fig. 5. However, the other schemes perform differently than the behavior observed in Fig. 5 for the power-law path-loss model. Specifically, the
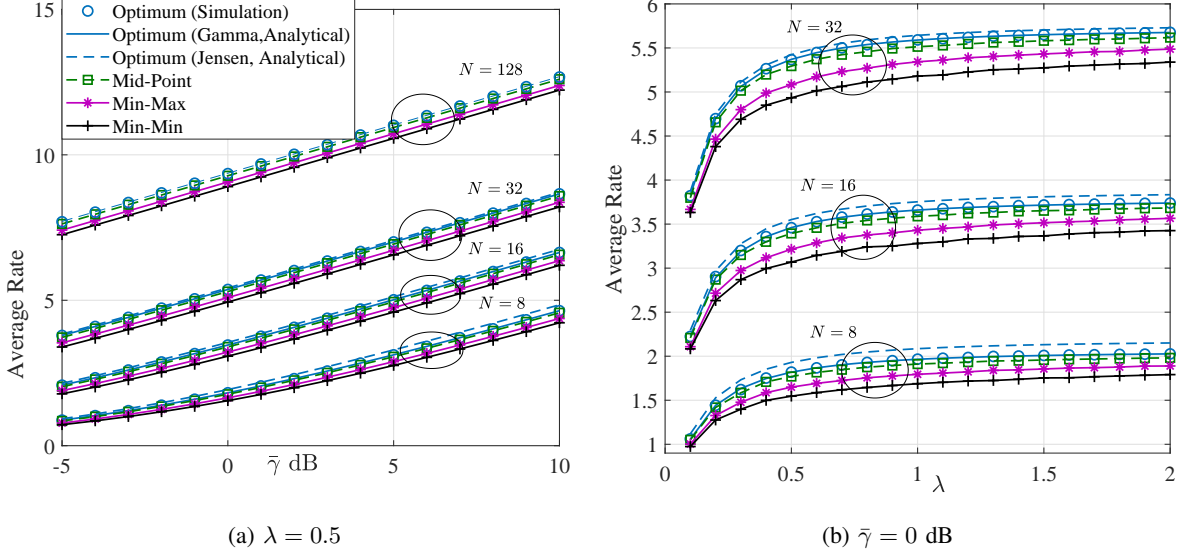
(a) $\lambda = 0.5$ (b) $\bar{\gamma} = 0$ dB

Fig. 8: Average rate achieved by different RIS selection schemes for different values of N, $d = 1.2$, $\alpha = 1.037$, for the exp-law path-loss model.

mid-point scheme always has very close performance with the optimum scheme. For example, the optimum scheme can save around 10% transmit power with respect to mid-point scheme to achieve the outage probability level of 10^{-3}. Min-min and min-max have the worst performance among these four schemes, where min-min starts to outperform min-max when SNR increases. In Fig. 7b, we see a significant outage performance increase when the density increases and the performance gap among the different schemes increases with the density, as we observed in Fig. 5b. In Fig. 7b, we also see that the performance advantage achieved by the optimum scheme over the mid-point scheme is minor when the density $\lambda = 0.1$. This means that the mid-point scheme is a near suboptimum selection scheme when the density is very small.

In Fig. 8, we plot the average rate versus the average SNR (i.e., see Fig. 8a) and the average rate versus density λ (i.e., see Fig. 8b). Analytical values calculated from (26) overlap with the simulation results, which verifies (26). Interestingly, we see that the optimum and mid-point selection schemes have very small rate differences for both $N = 16$ and 32 at $\lambda = 0.5$. For example, the rate difference is around 0.07 [bits/sec/Hz] for $N = 16$ at $\text{SNR} = 5\,\text{dB}$. For all three cases $N = 8, 16, 32$ in Fig. 8b, we have significant rate improvement from $\lambda = 0.1$ to $\lambda = 0.5$, and then there is a rate floor when λ increases further. This is due to the fact that there is a sufficient number of RISs within the neighborhood of TX and RX to support the communication. Thus, it is not worth to densify RISs in a given area beyond a certain limit.

(a) Power-Law: $\eta = 4$

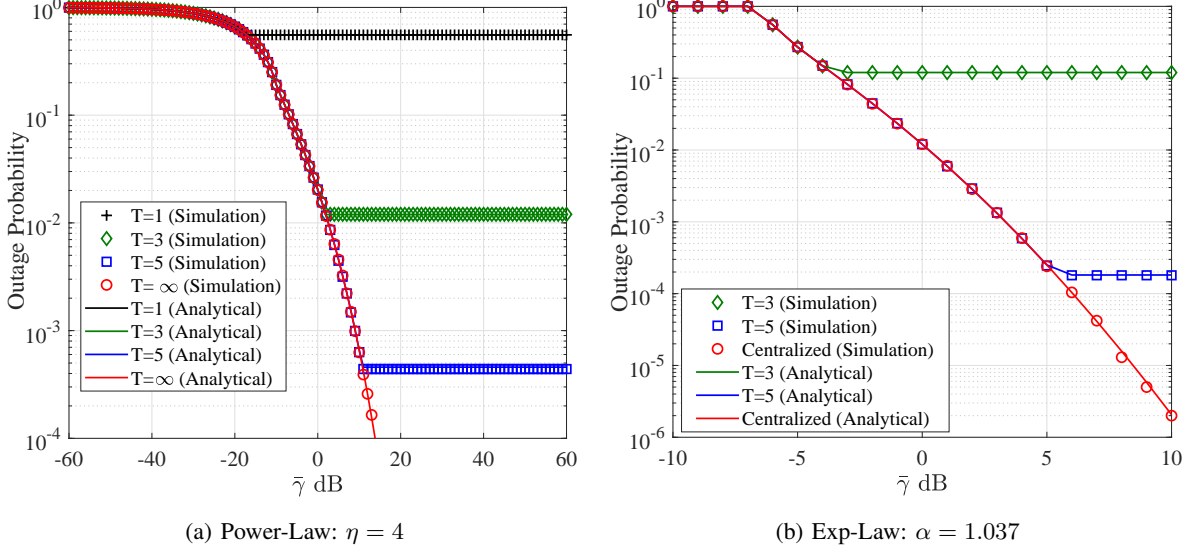(b) Exp-Law: $\alpha = 1.037$

Fig. 9: Outage probability achieved by limited-feedback RIS selection versus the average SNR $\bar{\gamma}$ for different values of the threshold T. $d = 1.2$, $N = 16$, $\lambda = 0.5$, and $\rho = 5$ dB.

B. Distributed Network Operation and Limited-Feedback Case

In Fig. 9, we plot the outage probability achieved by limited-feedback RIS selection versus the average SNR $\bar{\gamma}$ for the power-law model (Fig. 9a) and for the exp-law model (Fig. 9b). The analytical curves in Figs. 9a and 9b are obtained by (31) and (33), respectively. These curves perfectly match with simulations, thus validating the accuracy of (31) and (33). We do not consider $T = 1$ in Fig. 9b since there is no RIS feeding back when $T < 2d$ for the exp-law path-loss. In both figures, we see that outage probability curves first overlap with the centralized case and then keep constant as $\bar{\gamma}$ increases. This is because when $\bar{\gamma}$ is small, the values of target SNR satisfy the condition $\rho > \frac{\bar{\gamma}N(16+(N-1)\pi^2)}{T_{\text{pro}}^{\eta}16}$ for the power-law model and the condition $\rho > \frac{\bar{\gamma}N(16+(N-1)\pi^2)}{\exp(\alpha T_{\text{sum}})16}$ for the exp-law model. In such conditions, the outage performance is the same as the centralized case and does not depend on T since at least one RIS feeds its location information back to the source node. When $\bar{\gamma}$ continuously increases, these conditions are not satisfied and the outage probability does only depend on the average number of RISs feeding back, without any dependence on the average SNR and fading behavior. This is because the achieved outage probability depends on whether or not there is at least one RIS feeding its location information back to the source. We also see when T is larger, the outage performance is better in the flat region of outage curves. This is because when T is larger, we have a higher probability of at least one RIS feeding back, thus achieving better outage performance.

We plot the average rate for limited-feedback RIS selection versus $\bar{\gamma}$ for the power-law model in
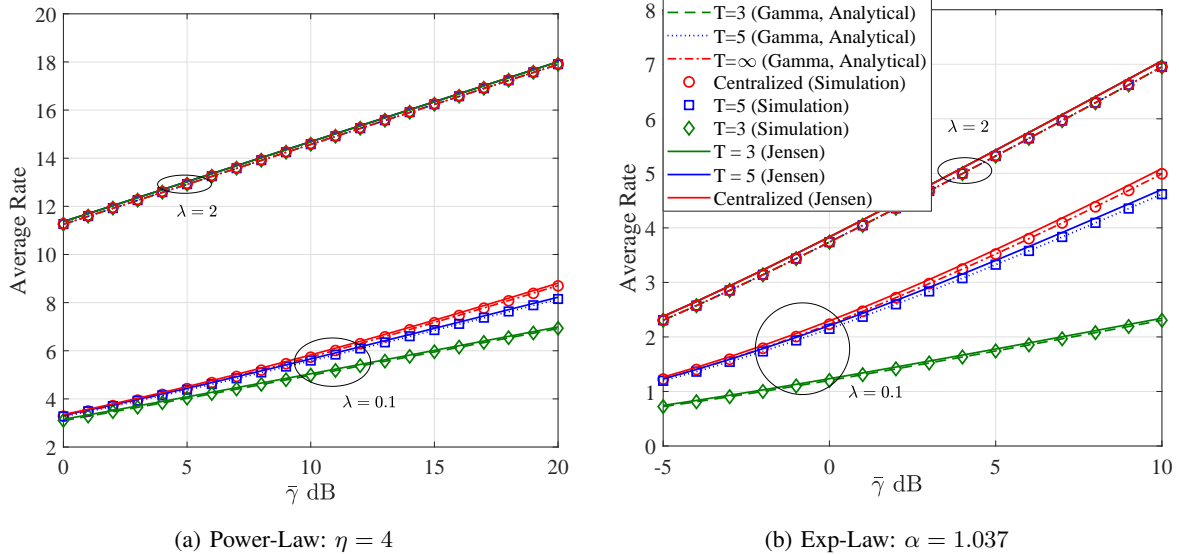
(a) Power-Law: $\eta = 4$

(b) Exp-Law: $\alpha = 1.037$

Fig. 10: Average rate achieved by limited-feedback RIS selection for different values of the threshold T. $d = 1.2$ and $N = 16$.

Fig. 10a and for the exp-law model in Fig. 10b. The perfect agreement between analytical curves obtained by (34) and (35) and simulations verify the accuracy of (34) and (35). For both Figs. 10a and 10b, we observe that for $\lambda = 0.1$, the performance loss from centralized case (which assumes the availability of location information from all RISs) to the case of $T = 5$ is much less than that from the case of $T = 5$ to that of $T = 3$. Based on (29), $T = 5$ leads to the average feedback load $\Xi_{\text{pro}} \approx 1.54$. This observation numerically demonstrates that small average feedback load around 1.54 is enough to experience negligible optimization loss, compared to the non-feedback case. This suggests that we can achieve a significant reduction in the feedback load in distributed network operation with limited-feedback, *whilst* not sacrificing from the data rate performance.

VI. CONCLUSION

In this paper, we have considered an RIS-aided wireless network where a single RIS is chosen from multiple PPP-distributed RISs to establish a communication link between the TX and RX. We have analyzed product-scaling and sum-scaling path-loss models in detail, which covers the important cases of RIS-aided end-to-end path-loss models. For each path-loss law, we have proposed an optimum location-based RIS selection policy which aims to maximize the network SNR and derived the distance distribution of the optimum RIS node location. Based on these distributions, we have evaluated the outage probability and the average rate of the optimum RIS selection policies to assess the network performance for the product-scaling and sum-scaling path-loss models. To make the network operation

distributed, we have further assumed the extra feedback capability at RISs and proposed limited-feedback RIS selection policies. We have derived the outage probabilities and average rates achieved by limited-feedback RIS selection policies for both path-loss models by deriving the distribution of the number of RISs feeding back. Our numerical results show the performance advantage of the proposed optimum and limited feedback RIS selection policies and reveal the performance gap for sub-optimum policies for product-scaling and sum-scaling path-loss models. Furthermore, the impact of system parameters, e.g., the number of reflecting elements and RIS node density, on the network performance have been quantified thoroughly by means of a comprehensive numerical analysis utilizing the derived analytical results.

Interesting future work includes considering the mixture product and sum scaling path-loss models for all RISs in a PPP and analyzing the performance metrics of the optimum selection policies under the mixture path-loss models. This work is an open problem since there are no completely consistent conditions to determine the regime where the product-scaling law holds and the regime where the sum-scaling law holds. Existing work, e.g., [26], [31], derive the path-loss under different setups and assumptions. Moreover, some conditions for determining these regimes and path-loss functions in [26], [31] do not have straightforward relationships with the TX-RIS and RIS-RX distances. This consequently makes it very challenging to analytically derive the performance metrics of optimum RIS selection policies where potential RISs have mixture path-loss models using the available path-loss models in the current literature. This problem may become tractable when easy-to-use conditions and path-loss expressions for the product-scaling and sum-scaling laws are available.

APPENDIX A

PROOF OF THEOREM 1

We first present an important lemma that lays the foundations for proving Theorem 1. This lemma will also be used in Appendix C for proving Theorem 3 as well.

Lemma 1: We denote $\mathcal{B}_{\text{right}}(\mathbf{0}, \tau)$ as the right half disc having non-negative first coordinates with radius τ centered at the origin $\mathbf{0}$. We assume that $\boldsymbol{U}_{\text{r}}$ is a uniformly distributed random node over $\mathcal{B}_{\text{right}}(\mathbf{0}, \tau)$. Let also $\Upsilon = \widehat{s}_{\text{pro}}(\boldsymbol{U}_{\text{r}})$. The expression for the CDF of RV Υ, $F_{\Upsilon}(\gamma)$, is given by (A.1).

Proof: By using the law of cosines, Υ can be written as

$$
\begin{aligned}
\Upsilon &= \sqrt{\left(\|\boldsymbol{U}_{\text{r}}\|^2 + 2d\,\|\boldsymbol{U}_{\text{r}}\|\cos\Theta + d^2\right)\left(\|\boldsymbol{U}_{\text{r}}\|^2 - 2d\,\|\boldsymbol{U}_{\text{r}}\|\cos\Theta + d^2\right)} \\
&= \sqrt{d^4 + \|\boldsymbol{U}_{\text{r}}\|^4 - 2d^2\|\boldsymbol{U}_{\text{r}}\|^2\cos 2\Theta}, \hspace{4em} \text{(A.2)}
\end{aligned}
$$

$$F_\Upsilon(\gamma) = \begin{cases} \frac{2}{\pi\tau^2}\left(\frac{1}{d^2}\left(d^4 E(\frac{\gamma^2}{d^4}) + (\gamma^2 - d^4)K(\frac{\gamma^2}{d^4})\right)\right) & \text{if } \gamma \leq d^2 \\ \frac{2}{\pi\tau^2}\left(\gamma E(\frac{d^4}{\gamma^2})\right) & \text{if } d^2 < \gamma \leq \tau^2 - d^2 \\ \frac{2}{\pi\tau^2}\left(-\frac{d^2}{2}\sqrt{1 - \frac{(d^4 - \gamma^2 + \tau^4)^2}{4d^4\tau^4}} + \gamma E(\frac{d^4}{\gamma^2}) - \frac{\gamma E(\arccos(\frac{d^4+\tau^4-\gamma^2}{2d^2\tau^2}), \frac{d^4}{\gamma^2})}{2} + \theta_2\tau^2\right); & \text{if } \tau^2 - d^2 < \gamma \leq d^2 + \tau^2 \\ 1 & \text{if } \gamma > d^2 + \tau^2 \end{cases}$$
$$\text{(A.1)}$$

where Θ is the angle between the non-negative x-axis and the line segment connecting $\mathbf{0}$ and $\boldsymbol{U}_\mathrm{r}$. Θ is uniformly distributed over $\left[-\frac{\pi}{2}, \frac{\pi}{2}\right]$, and is independent of $\|\boldsymbol{U}_\mathrm{r}\|$ because $\boldsymbol{U}_\mathrm{r}$ is uniformly distributed. Thus, we derive the conditional CDF of Υ given $\{\Theta = \theta\}$ as

$$F_{\Upsilon|\Theta}(\gamma|\theta) = \Pr\left\{\Upsilon^2 \leq \gamma^2|\Theta = \theta\right\} = \Pr\left\{d^4 + \|\boldsymbol{U}_\mathrm{r}\|^4 - 2d^2\|\boldsymbol{U}_\mathrm{r}\|^2\cos 2\theta \leq \gamma^2|\Theta = \theta\right\}. \quad \text{(A.3)}$$

To solve (A.3), we study the monotonicity of the function $f(\|\boldsymbol{U}_\mathrm{r}\|) = d^4 + \|\boldsymbol{U}_\mathrm{r}\|^4 - 2d^2\|\boldsymbol{U}_\mathrm{r}\|^2\cos 2\theta$. We obtain the first derivative of $f(\|\boldsymbol{U}_\mathrm{r}\|)$ with respect to $\|\boldsymbol{U}_\mathrm{r}\|$ as $f'(\|\boldsymbol{U}_\mathrm{r}\|) = 4\|\boldsymbol{U}_\mathrm{r}\|^3 - 4d^2\|\boldsymbol{U}_\mathrm{r}\|\cos 2\theta$. Based on the expression of $f'(\|\boldsymbol{U}_\mathrm{r}\|)$, we find that $f'(\|\boldsymbol{U}_\mathrm{r}\|) > 0$ holds when the case 1) $\cos 2\theta \leq 0$ and $\|\boldsymbol{U}_\mathrm{r}\| > 0$ or case 2) $\cos 2\theta > 0$ and $\|\boldsymbol{U}_\mathrm{r}\| > \sqrt{d^2\cos 2\theta}$ is satisfied. That is to say, for $\theta \in \left[\frac{\pi}{4}, \frac{\pi}{2}\right] \cup \theta \in \left[-\frac{\pi}{2}, -\frac{\pi}{4}\right]$, $f(\|\boldsymbol{U}_\mathrm{r}\|)$ is an increasing function with $\|\boldsymbol{U}_\mathrm{r}\|$. For $\theta \in \left[-\frac{\pi}{4}, \frac{\pi}{4}\right]$, $f(\|\boldsymbol{U}_\mathrm{r}\|)$ is an increasing function when $\|\boldsymbol{U}_\mathrm{r}\| > \sqrt{d^2\cos 2\theta}$ and $f(\|\boldsymbol{U}_\mathrm{r}\|)$ is a decreasing function when $\|\boldsymbol{U}_\mathrm{r}\| < \sqrt{d^2\cos 2\theta}$.

We first solve (A.3) for $\theta \in \left[\frac{\pi}{4}, \frac{\pi}{2}\right] \cup \left[-\frac{\pi}{2}, -\frac{\pi}{4}\right]$. Under these conditions, only one positive root U_1 for $f(\|\boldsymbol{U}_\mathrm{r}\|) - \gamma^2 = 0$ exists, which is given by

$$U_1 = \sqrt{-d^2 + 2d^2\cos^2\theta + \frac{\sqrt{-d^4 + 2\gamma^2 + d^4\cos 4\theta}}{\sqrt{2}}}. \quad \text{(A.4)}$$

Since $0 \leq \|\boldsymbol{U}_\mathrm{r}\| \leq \tau$ and $f(\|\boldsymbol{U}_\mathrm{r}\|)$ is an increasing function with $\|\boldsymbol{U}_\mathrm{r}\|$, thus we obtain $d^4 \leq f(\|\boldsymbol{U}_\mathrm{r}\|) \leq d^4 + \tau^4 - 2d^2\tau^2\cos 2\theta$. Given U_1 and the range of $f(\|\boldsymbol{U}_\mathrm{r}\|)$, we solve (A.3) for $\theta \in \left[\frac{\pi}{4}, \frac{\pi}{2}\right] \cup \left[-\frac{\pi}{2}, -\frac{\pi}{4}\right]$ as

$$F_{\Upsilon|\Theta}\left(\gamma|\theta, \theta \in \left[\frac{\pi}{4}, \frac{\pi}{2}\right] \cup \left[-\frac{\pi}{2}, -\frac{\pi}{4}\right]\right) = \begin{cases} 0 & \text{if } \gamma < d^2 \\ \Pr\{\|\boldsymbol{U}_\mathrm{r}\| \leq U_1\} = \frac{U_1^2}{\tau^2} & \\ & \text{if } d^2 \leq \gamma \leq \sqrt{d^4 + \tau^4 - 2d^2\tau^2\cos 2\theta} \\ 1 & \text{if } \gamma > \sqrt{d^4 + \tau^4 - 2d^2\tau^2\cos 2\theta} \end{cases} \quad \text{(A.5)}$$

where $\Pr\{\|\boldsymbol{U}_\mathrm{r}\| \leq U_1\} = \frac{U_1^2}{\tau^2}$ is based on the CDF of $\|\boldsymbol{U}_\mathrm{r}\|$, i.e., $F_{\|\boldsymbol{U}_\mathrm{r}\|}(u) = \frac{u^2}{\tau^2}$.

We next solve (A.3) for $\theta \in \left[-\frac{\pi}{4}, \frac{\pi}{4}\right]$. Under these conditions, two positive roots U_1 and U_2 for $f(\|\boldsymbol{U}_{\mathrm{r}}\|) - \gamma^2 = 0$ exist, where U_1 is given by (A.4) and U_2 is given by

$U_2 = \sqrt{-d^2 + 2d^2\cos^2\theta - \frac{\sqrt{-d^4 + 2\gamma^2 + d^4\cos 4\theta}}{\sqrt{2}}}$. Since $f(\|\boldsymbol{U}_{\mathrm{r}}\|)$ is an increasing function when $(\|\boldsymbol{U}_{\mathrm{r}}\|) > \sqrt{d^2\cos 2\theta}$ and $f(\|\boldsymbol{U}_{\mathrm{r}}\|)$ is a decreasing function when $(\|\boldsymbol{U}_{\mathrm{r}}\|) < \sqrt{d^2\cos 2\theta}$, $f(\|\boldsymbol{U}_{\mathrm{r}}\|)$ attains the minimal value $f\left(\sqrt{d^2\cos 2\theta}\right) = d^4 - d^4\cos^2 2\theta$ at $\|\boldsymbol{U}_{\mathrm{r}}\| = \sqrt{d^2\cos 2\theta}$. Thus, the range of $f(\|\boldsymbol{U}_{\mathrm{r}}\|)$ is $d^4 - d^4\cos^2 2\theta \le f(\|\boldsymbol{U}_{\mathrm{r}}\|) \le d^4 + \tau^4 - 2d^2\tau^2\cos 2\theta$. Given U_1, U_2, and the range of $f(\|\boldsymbol{U}_{\mathrm{r}}\|)$, we solve (A.3) when $\theta \in \left[-\frac{\pi}{4}, \frac{\pi}{4}\right]$ as

$$F_{\Upsilon|\Theta}\left(\gamma|\theta, \theta \in \left[-\frac{\pi}{4}, \frac{\pi}{4}\right]\right) = \begin{cases} 0 & \text{if } \gamma < \sqrt{d^4 - d^4\cos^2 2\theta} \\ \Pr\{U_2 \le \|\boldsymbol{U}_{\mathrm{r}}\| \le U_1\} = \frac{U_1{}^2 - U_2{}^2}{\tau^2} \\ \quad \text{if } \sqrt{d^4 - d^4\cos^2 2\theta} \le \gamma \le d^2 \\ \Pr\{\|\boldsymbol{U}_{\mathrm{r}}\| \le U_1\} = \frac{U_1{}^2}{\tau^2} \\ \quad \text{if } d^2 \le \gamma \le \sqrt{d^4 + \tau^4 - 2d^2\tau^2\cos 2\theta} \\ 1 & \text{if } \gamma > \sqrt{d^4 + \tau^4 - 2d^2\tau^2\cos 2\theta} \end{cases} \tag{A.6}$$

We will obtain $F_\Upsilon(\gamma)$ by averaging $F_{\Upsilon|\Theta}(\gamma|\theta)$ over Θ. For $\theta \in \left[\frac{\pi}{4}, \frac{\pi}{2}\right] \cup \left[-\frac{\pi}{2}, -\frac{\pi}{4}\right]$, we have

$$F_\Upsilon\left(\gamma|\theta \in \left[\frac{\pi}{4}, \frac{\pi}{2}\right] \cup \left[-\frac{\pi}{2}, -\frac{\pi}{4}\right]\right) = \begin{cases} 0 & \text{if } \gamma < d^2 \\ \frac{2}{\pi}\left(\int_{\frac{\pi}{4}}^{\frac{\pi}{2}} \frac{U_1{}^2}{\tau^2} d\theta\right) & \text{if } d^2 \le \gamma \le \sqrt{d^4 + \tau^4} \\ \frac{2}{\pi\tau^2}\left(\int_{\theta_2}^{\frac{\pi}{2}} U_1{}^2 d\theta + \int_{\frac{\pi}{4}}^{\theta_2} \tau^2 d\theta\right) & \text{if } \sqrt{d^4 + \tau^4} \le \gamma \le d^2 + \tau^2 \\ \frac{2}{\pi\tau^2}\left(\int_{\frac{\pi}{2}}^{\frac{\pi}{4}} \tau^2 d\theta\right) & \text{if } \gamma \ge d^2 + \tau^2 \end{cases} \tag{A.7}$$

For $\theta \in \left[-\frac{\pi}{4}, \frac{\pi}{4}\right]$, we have

$$F_\Upsilon\left(\gamma|\theta \in \left[-\frac{\pi}{4}, \frac{\pi}{4}\right]\right) = \begin{cases} \frac{2}{\pi}\left(\int_{\theta_1}^{\frac{\pi}{4}} 0\, d\theta + \int_0^{\theta_1} \frac{U_1{}^2 - U_2{}^2}{\tau^2} d\theta\right) & \text{if } \gamma < d^2 \\ \frac{2}{\pi}\left(\int_0^{\frac{\pi}{4}} \frac{U_1{}^2}{\tau^2} d\theta\right) & \text{if } d^2 \le \gamma \le \sqrt{\tau^2 - d^2} \\ \frac{2}{\pi}\left(\int_{\theta_2}^{\frac{\pi}{4}} \frac{U_1{}^2}{\tau^2} d\theta + \int_0^{\theta_2} 1\, d\theta\right) & \text{if } \tau^2 - d^2 \le \gamma \le \sqrt{d^4 + \tau^4} \\ \frac{2}{\pi}\left(\int_0^{\frac{\pi}{4}} 1\, d\theta\right) & \text{if } \gamma \ge \sqrt{d^4 + \tau^4} \end{cases} \tag{A.8}$$

Combining (A.7) and (A.8), for $\theta \in \left[-\frac{\pi}{2}, \frac{\pi}{2}\right]$, we have

$$F_\Upsilon\left(\gamma|\theta \in \left[-\frac{\pi}{2}, \frac{\pi}{2}\right]\right) = \begin{cases} \frac{2}{\pi}\left(\int_0^{\theta_1} \frac{U_1{}^2 - U_2{}^2}{\tau^2} d\theta\right) & \text{if } \gamma < d^2 \\ \frac{2}{\pi}\left(\int_0^{\frac{\pi}{4}} \frac{U_1{}^2}{\tau^2} d\theta + \int_{\frac{\pi}{4}}^{\frac{\pi}{2}} \frac{U_1{}^2}{\tau^2} d\theta\right) & \text{if } d^2 \le \gamma \le \tau^2 - d^2 \\ \frac{2}{\pi}\left(\int_{\theta_2}^{\frac{\pi}{4}} \frac{U_1{}^2}{\tau^2} d\theta + \int_0^{\theta_2} 1\, d\theta + \int_{\frac{\pi}{4}}^{\frac{\pi}{2}} \frac{U_1{}^2}{\tau^2} d\theta\right) & \text{if } \tau^2 - d^2 \le \gamma \le \sqrt{d^4 + \tau^4} \\ \frac{2}{\pi}\left(\int_0^{\frac{\pi}{4}} 1\, d\theta + \int_{\theta_2}^{\frac{\pi}{2}} \frac{U_1{}^2}{\tau^2} d\theta + \int_{\frac{\pi}{4}}^{\theta_2} 1\, d\theta\right) & \text{if } \sqrt{d^4 + \tau^4} \le \gamma \le d^2 + \tau^2 \\ \frac{2}{\pi}\left(\int_0^{\frac{\pi}{4}} 1\, d\theta + \int_{\frac{\pi}{4}}^{\frac{\pi}{2}} 1\, d\theta\right) & \text{if } \gamma \ge d^2 + \tau^2 \end{cases} \tag{A.9}$$

Applying [42, eq. (2.576)] given by $\int \sqrt{a+b\cos x}\,dx = \frac{2}{b}\left((a-b)F(c_1, \frac{1}{c_2}) + 2bE(c_1, \frac{1}{c_2})\right)$ and applying $\int \sqrt{a+b\cos x}\,dx = 2\sqrt{a+b}E(\frac{x}{2}, c_1)$ to (A.9), where $c_1 = \arcsin\sqrt{\frac{b(1-\cos x)}{a+b}}$ and $c_2 = \sqrt{\frac{2b}{a+b}}$, we obtain $F_\Upsilon(\gamma)$ as in (A.1) in Lemma 1. The proof of Lemma 1 ends here. Finally, using the relation $F_{\Upsilon_{\text{opt}}}(\gamma) = 1 - \left(\lim_{\tau\to\infty} \exp\left(-\frac{\lambda\pi\tau^2}{2} F_\Upsilon(\gamma)\right)\right)^2$ given by [28] and the result of $F_\Upsilon(\gamma)$ given in Lemma 1, we arrive at (8), which concludes the proof. ∎

APPENDIX B

PROOF OF THEOREM 2

We assume $\boldsymbol{U}_\text{r}$ is a uniformly distributed random RIS location. We also assume that $\Lambda = \widehat{s}_\text{sum}(\boldsymbol{U}_\text{r})$, which is the sum of the distance between the source node and $\boldsymbol{U}_\text{r}$ and the distance between $\boldsymbol{U}_\text{r}$ and the destination node. By using the law of cosines, we write Λ as

$$\Lambda = \sqrt{\|\boldsymbol{U}_\text{r}\|^2 + 2d\|\boldsymbol{U}_\text{r}\|\cos\Theta + d^2} + \sqrt{\|\boldsymbol{U}_\text{r}\|^2 - 2d\|\boldsymbol{U}_\text{r}\|\cos\Theta + d^2} \tag{B.1}$$

The conditional CDF of Λ given $\{\Theta = \theta\}$ can be expressed as

$$F_{\Lambda|\Theta}(\gamma|\theta) = \Pr\left\{\Lambda^2 \leq \gamma^2 | \Theta = \theta\right\} = \Pr\left\{w(\|\boldsymbol{U}_\text{r}\|) \leq \gamma^2 | \Theta = \theta\right\}, \tag{B.2}$$

where

$$w(\|\boldsymbol{U}_\text{r}\|) = 2d^2 + 2\|\boldsymbol{U}_\text{r}\|^2 + \sqrt{\left(\|\boldsymbol{U}_\text{r}\|^2 + 2d\|\boldsymbol{U}_\text{r}\|\cos\theta + d^2\right)\left(\|\boldsymbol{U}_\text{r}\|^2 - 2d\|\boldsymbol{U}_\text{r}\|\cos\theta + d^2\right)}. \tag{B.3}$$

We note that only one positive root W_1 for $w(\|\boldsymbol{U}_\text{r}\|) - \gamma^2 = 0$ exist, where W_1 is given by

$$W_1 = \frac{\sqrt{-4d^2\gamma^2 + \gamma^4}}{2\sqrt{\gamma^2 - 4d^2\cos^2\theta}}. \tag{B.4}$$

Based on $w(\|\boldsymbol{U}_\text{r}\|)$ is the increasing function with respect to $\|\boldsymbol{U}_\text{r}\|$ and $0 \leq \|\boldsymbol{U}_\text{r}\| \leq \tau$, we obtain the range of $w(\|\boldsymbol{U}_\text{r}\|)$ is $4d^2 \leq w(\|\boldsymbol{U}_\text{r}\|) \leq w(\tau)$. Given W_1 and the range of $w(\|\boldsymbol{U}_\text{r}\|)$, we solve (B.2) as

$$F_{\Lambda|\Theta}(\gamma|\theta) = \begin{cases} 0 & \text{if } \gamma < 2d \\ \Pr\{\|\boldsymbol{U}_\text{r}\| \leq W_1\} = \frac{W_1^2}{\tau^2} & \text{if } 2d \leq \gamma \leq \sqrt{w(\tau)} \\ 1 & \text{if } \gamma > \sqrt{w(\tau)} \end{cases} \tag{B.5}$$

We will obtain $F_\Lambda(\gamma)$ by averaging $F_{\Omega|\Theta}(\gamma|\theta)$ over Θ. We need to consider four cases separately, as follows:

$$F_\Lambda(\gamma) = \begin{cases} 0 & \text{if } \gamma \leq 2d \\ \frac{2}{\pi\tau^2}\int_0^{\frac{\pi}{2}} W_1^2\,d\theta & \text{if } 2d < \gamma \leq 2\tau \\ \frac{2}{\pi\tau^2}\int_{\phi_1}^{\frac{\pi}{2}} W_1^2\,d\theta + \frac{2}{\pi}\int_0^{\phi_1} 1\,d\theta & \text{if } 2\tau < \gamma \leq 2\sqrt{d^2 + \tau^2} \\ 1 & \text{if } \gamma > 2\sqrt{d^2 + \tau^2} \end{cases}, \tag{B.6}$$

$$F_\Lambda(\gamma) = \begin{cases} 0 & \text{if } \gamma \leq 2d \\ \frac{2}{\pi\tau^2}\left(\frac{1}{8}(-1)^{\left\lfloor \frac{\pi - 2\mathrm{Arg}(\gamma)+\mathrm{Arg}\left(-4d^2+\gamma^2\right)}{2\pi}\right\rfloor}\pi\gamma\sqrt{-4d^2+\gamma^2}\right) & \text{if } 2d < \gamma \leq 2\tau \\ \frac{2}{\pi\tau^2}\left(-\frac{\arctan\left(\cot(\theta)\sqrt{\frac{-4d^2+\gamma^2}{\gamma^2}}\right)\sqrt{\gamma^2(-4d^2+\gamma^2)}}{4}+\phi_1\tau^2\right) & \text{if } 2\tau < \gamma \leq 2\sqrt{d^2+\tau^2} \\ 1 & \text{if } \gamma > 2\sqrt{d^2+\tau^2} \end{cases} \tag{B.7}$$

where $\phi_1 = \frac{1}{2}\arccos\left(\frac{d^4+\tau^4-\frac{\left(\gamma^2-2d^2-2\tau^2\right)^2}{4}}{2d^2\tau^2}\right)$ and ϕ_1 is obtained by solving $\gamma^2 = w(\tau)$. Applying [39, eq. (2.562.2)], we obtain $F_\Lambda(\gamma)$ as in (B.7). Using $F_{\Lambda_{\mathrm{opt}}}(\gamma) = 1 - \left(\lim_{\tau\to\infty}\exp\left(-\frac{\lambda\pi\tau^2}{2}F_\Lambda(\gamma)\right)\right)^2$ [28], we arrive at (10). This completes the proof.

APPENDIX C

PROOF OF THEOREM 3

We denote $\mathcal{B}(\mathbf{0},\tau)$ as the disc centered at the origin $\mathbf{0}$ with radius τ. We assume $\Xi_{\mathrm{pro}}(\tau)$ as the average number of RISs located in $\mathcal{B}(\mathbf{0},\tau)$ that feedback their channel quality indicators. We also assume that $\boldsymbol{U}$ is a uniformly distributed random node over $\mathcal{B}(\mathbf{0},\tau)$. Thus, we have

$$\Xi_{\mathrm{pro}}(\tau) = \lambda\pi\tau^2 \mathsf{Pr}\left\{\widehat{s}_{\mathrm{pro}}(\boldsymbol{U}) \leq T_{\mathrm{pro}}\right\}. \tag{C.1}$$

We next obtain $\mathsf{Pr}\left\{\widehat{s}_{\mathrm{pro}}(\boldsymbol{U}) \leq T_{\mathrm{pro}}\right\}$. We recall that $\boldsymbol{U}_{\mathrm{r}}$ is defined in Lemma 1 and $\boldsymbol{U}_{\mathrm{r}}$ is a uniformly distributed random node over right half disc $\mathcal{B}_{\mathrm{right}}(\mathbf{0},\tau)$. Similarly, we define $\mathcal{B}_{\mathrm{left}}(\mathbf{0},\tau)$ as the left half disc that centered at the origin $\mathbf{0}$ with radius τ having negative first coordinates. We let $\boldsymbol{U}_{\mathrm{l}}$ is a uniformly distributed random node over left half disc $\mathcal{B}_{\mathrm{left}}(\mathbf{0},\tau)$.

Since the distribution of $\boldsymbol{U}_{\mathrm{r}}$ over $\mathcal{B}_{\mathrm{right}}$ is same as the distribution of $\boldsymbol{U}_{\mathrm{l}}$ over $\mathcal{B}_{\mathrm{left}}$, $\boldsymbol{U}$, $\boldsymbol{U}_{\mathrm{r}}$, and $\boldsymbol{U}_{\mathrm{l}}$ are identically distributed RVs. As such, we have

$$\mathsf{Pr}\left\{\widehat{s}_{\mathrm{pro}}(\boldsymbol{U}) \leq T_{\mathrm{pro}}\right\} = \mathsf{Pr}\left\{\widehat{s}_{\mathrm{pro}}(\boldsymbol{U}_{\mathrm{r}}) \leq T_{\mathrm{pro}}\right\} = \mathsf{Pr}\left\{\widehat{s}_{\mathrm{pro}}(\boldsymbol{U}_{\mathrm{l}}) \leq T_{\mathrm{pro}}\right\}. \tag{C.2}$$

We note that the CDF of Υ, $F_\Upsilon(\gamma)$, is given by (A.1), where $\Upsilon = \widehat{s}_{\mathrm{pro}}(\boldsymbol{U}_{\mathrm{r}})$. Thus, the expression for $\mathsf{Pr}\left\{\widehat{s}_{\mathrm{pro}}(\boldsymbol{U}) \leq T_{\mathrm{pro}}\right\}$ can be obtained by replacing γ with T_{pro} in (A.1). Finally, applying the expression for $\mathsf{Pr}\left\{\widehat{s}_{\mathrm{pro}}(\boldsymbol{U}) \leq T_{\mathrm{pro}}\right\}$ to (C.1) and taking the limit $\Xi_{\mathrm{pro}} = \lim_{\tau\to}\Xi_{\mathrm{pro}}(\tau)$, we arrive at (29). The Poisson distribution property for the number of RISs feeding back can be established by using characteristic functions as in [28], which completes the proof.

APPENDIX D

SIMULATIONS WITH MIXTURE PATH-LOSS MODELS

In this appendix, we conduct simulations with mixture product-scaling and sum-scaling path-loss models and compare these simulations with our analysis with a single path-loss models for all potential RISs, to show the reasonableness of the used assumption. We recall that [26] shows the path-loss is product-scaling if the TX and RX are both in the far-field of RIS in the beamforming case and shows the path-loss is sum-scaling if the TX and RX are both or only one of them in the near-field of RIS, in the broadcasting case. Based on the conditions where product-scaling and sum-scaling path-loss models hold in [26], in our simulations, we calculate the path-loss of each RIS using sum-scaling law if the TX and RX are both or only one of them in the near-field of RIS or using the product-scaling law if the TX and RX are both in the far-field of RIS. Fortunately, by conducting new simulations, we show that i) the results derived by assuming all RISs have the same sum-scaling path-loss model can be good approximations of the results that assumes mixture path-loss models for large RISs, and ii) the results assuming all RISs have the same product-scaling path-loss model can be good approximations of the results assuming mixture path-loss models for small RISs. Please see the results below:
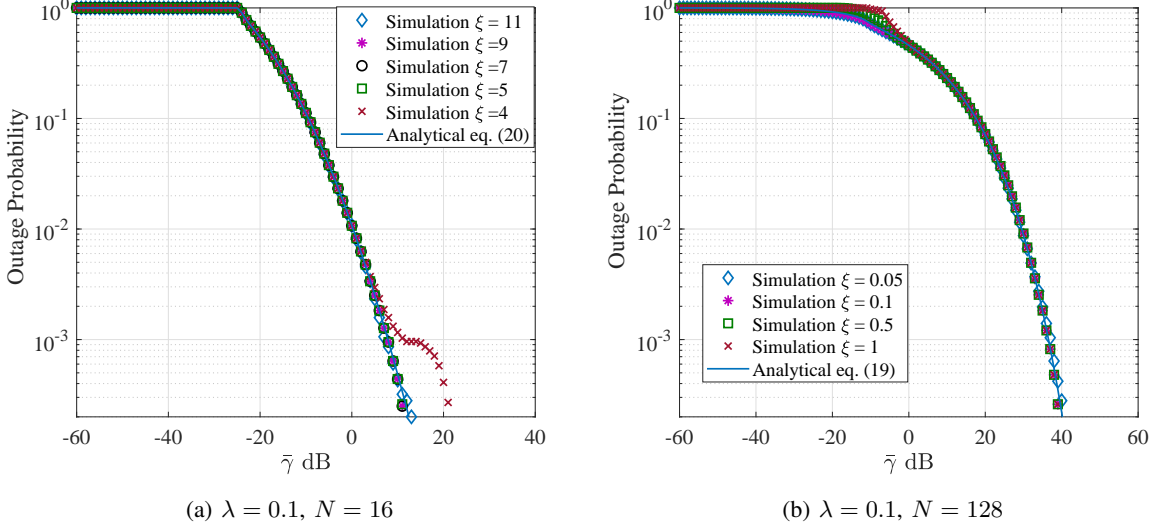

(a) $\lambda = 0.1$, $N = 16$ (b) $\lambda = 0.1$, $N = 128$

Fig. 11: In simulations, the path-loss of RIS-aided links follow the power-law path-loss model if the RIS located at $\boldsymbol{X}_i$ satisfy $\|\boldsymbol{x}_s - \boldsymbol{X}_i\| > \xi$ and $\|\boldsymbol{X}_i - \boldsymbol{x}_d\| > \xi$; otherwise, RIS-aided links follow the exp-law path-loss model. $\xi = \frac{8L_x L_y}{\lambda_s}$ is the boundary of the far-field and near-field defined in [26] and other parameters are the same as those in the manuscript.

In Fig. 11a, we observe that the simulations with the boundary values of $\xi = 5, 7, 9, 11$ have a good agreement with (20). This means the analytical outage probability with the sum-scaling law is a good approximation of the simulated outage probability with product-scaling and sum-scaling path-loss models co-existing for potential RISs, when the boundary value ξ is relatively large, e.g., $\xi \geq 5$. This is because the RISs in the regime of product-scaling path-loss model (i.e., the TX and RX are both in the far-field of the RIS) are less likely to be the optimum one compared with the RISs in the regime of sum-scaling path-loss model (i.e., the TX and RX are both or only one of them in the near-field of RIS). This likelihood decreases when the boundary value ξ of the far-field and near-field increases. We note that $\xi \geq 5$ is the normal range values of ξ of electrically-large RISs. For example, [26] considers one large RIS prototype with the size of $1\,\mathrm{m} \times 1.2\,\mathrm{m}$ and another large RIS prototype with the size of $0.34\,\mathrm{m} \times 0.5\,\mathrm{m}$, and carrier frequency is 10.5 GHz, which leads to $\xi = 71.4\,\mathrm{m}$ and $\xi = 11.9\,\mathrm{m}$. In Fig. 11b, we observe that the simulations with the boundary values of $\xi = 0.05, 0.1$ have a good agreement with (19). This means the analytical outage probability with the product-scaling law is a good approximation of the simulated outage probability with product-scaling and sum-scaling path-loss models co-existing for potential RISs, when the boundary value ξ is relatively small, e.g., $\xi \leq 0.1$. This is because most of RISs are in the regime of product-scaling path-loss model, i.e., the TX and RX are both in the far-field of most of RISs, when ξ is small. We note that $\xi \leq 0.1$ is the normal range values of ξ of electrically-small RISs. For example, [26] considers a small RIS prototype with the size of $0.384\,\mathrm{m} \times 0.096\,\mathrm{m}$, which leads to $\xi = 0.1\,\mathrm{m}$ when the carrier frequency is 425 MHz.

REFERENCES

[1] The Radiocommunication Sector of ITU, "IMT traffic estimates for the years 2020 to 2030," Tech. Rep., Jul. 2015.

[2] M. D. Renzo *et al.*, "Smart radio environments empowered by AI reconfigurable meta-surfaces: An idea whose time has come," *EURASIP J. Wireless Commun. Netw.*, vol. 2019:129, May 2019.

[3] J. Hu *et al.*, "Reconfigurable intelligent surface based RF sensing: Design, optimization, and implementation," *IEEE J. Select. Areas Commun.*, vol. 38, no. 11, pp. 2700–2716, Nov. 2020.

[4] L. Dai *et al.*, "Reconfigurable intelligent surface-based wireless communications: Antenna design, prototyping, and experimental results," *IEEE Access*, vol. 8, pp. 45 913–45 923, Mar. 2020.

[5] C. Huang, A. Zappone, G. C. Alexandropoulos, M. Debbah, and C. Yuen, "Reconfigurable intelligent surfaces for energy efficiency in wireless communication," *IEEE Trans. Wireless Commun.*, vol. 18, no. 8, pp. 4157–4170, Aug. 2019.

[6] M. Jung, W. Saad, Y. Jang, G. Kong, and S. Choi, "Performance analysis of large intelligent surfaces (LISs): Asymptotic data rate and channel hardening effects," *IEEE Trans. Wireless Commun.*, vol. 19, no. 3, pp. 2052–2065, Mar. 2020.

[7] J. He, K. Yu, and Y. Shi, "Coordinated passive beamforming for distributed intelligent reflecting surfaces network," in *Proc. IEEE VTC-Spring*, May 2020, pp. 1–5.

[8] Y. Xiu, J. Zhao, C. Yuen, Z. Zhang, and G. Gui, "Secure beamforming for distributed intelligent reflecting surfaces aided mmWave systems," 2020. [Online]. Available: arXiv:2006.14851

[9] Z. Yang, M. Chen, W. Saad, W. Xu, M. Shikh-Bahaei, H. V. Poor, and S. Cui, "Energy-efficient wireless communications with distributed reconfigurable intelligent surfaces," *IEEE Trans. Wireless Commun.*, 2021, Early Access.

[10] B. Zheng, C. You, and R. Zhang, "Double-IRS assisted multi-user MIMO: Cooperative passive beamforming design," *IEEE Trans. Wireless Commun.*, vol. 20, no. 7, pp. 4513–4526, Feb. 2021.

[11] Y. Han, S. Zhang, L. Duan, and R. Zhang, "Cooperative double-irs aided communication: Beamforming design and power scaling," *IEEE Wireless Commun. Lett.*, vol. 9, no. 8, pp. 1206–1210, 2020.

[12] S. Zhang and R. Zhang, "Intelligent reflecting surface aided multi-user communication: Capacity region and deployment strategy," *IEEE Trans. Commun.*, vol. 69, no. 9, pp. 5790–5806, 2021.

[13] L. Wei, C. Huang, G. C. Alexandropoulos, C. Yuen, Z. Zhang, and M. Debbah, "Channel estimation for ris-empowered multi-user miso wireless communications," *IEEE Trans. Commun.*, vol. 69, no. 6, pp. 4144–4157, 2021.

[14] C. Huang, Z. Yang, G. C. Alexandropoulos, K. Xiong, L. Wei, C. Yuen, Z. Zhang, and M. Debbah, "Multi-hop ris-empowered terahertz communications: A drl-based hybrid beamforming design," *IEEE J. Select. Areas Commun.*, vol. 39, no. 6, pp. 1663–1677, 2021.

[15] W. Mei and R. Zhang, "Performance analysis and user association optimization for wireless network aided by multiple intelligent reflecting surfaces," *IEEE Trans. Commun.*, vol. 69, no. 9, pp. 6296–6312, Jun. 2021.

[16] L. Yang, Y. Yang, D. B. d. Costa, and I. Trigui, "Outage probability and capacity scaling law of multiple ris-aided networks," *IEEE Wireless Commun. Lett.*, vol. 10, no. 2, pp. 256–260, 2021.

[17] J. G. Andrews, F. Baccelli, and R. K. Ganti, "A tractable approach to coverage and rate in cellular networks," *IEEE Trans. Commun.*, vol. 59, no. 11, pp. 3122–3134, Nov. 2011.

[18] M. D. Renzo and J. Song, "Reflection probability in wireless networks with metasurface-coated environmental objects: An approach based on random spatial processes," *EURASIP J. Wireless Commun.*, no. 99, pp. 1–15, Apr. 2019.

[19] T. Hou, Y. Liu, Z. Song, X. Sun, Y. Chen, and L. Hanzo, "MIMO assisted networks relying on intelligent reflective surfaces: A stochastic geometry based analysis," *IEEE Transactions on Vehicular Technology*, vol. 71, no. 1, pp. 571–582, 2022.

[20] M. A. Kishk and M.-S. Alouini, "Exploiting randomly located blockages for large-scale deployment of intelligent surfaces," *IEEE J. Select. Areas Commun.*, vol. 39, no. 4, pp. 1043–1056, Apr. 2021.

[21] Y. Zhu, G. Zheng, and K. Wong, "Stochastic geometry analysis of large intelligent surface-assisted millimeter wave networks," *IEEE J. Select. Areas Commun.*, vol. 38, no. 8, pp. 1749–1762, Aug. 2020.

[22] M. Nemati, J. Park, and J. Choi, "RIS-assisted coverage enhancement in millimeter-wave cellular networks," *IEEE Access*, vol. 8, pp. 188 171–188 185, Oct. 2020.

[23] T. Shafique, H. Tabassum, and E. Hossain, "Stochastic geometry analysis of irs-assisted downlink cellular networks," *IEEE Trans. Commun.*, vol. 70, no. 2, pp. 1442–1456, 2022.

[24] C. Psomas, H. A. Suraweera, and I. Krikidis, "On the association with intelligent reflecting surfaces in spatially random networks," in *Proc. IEEE ICC*, May 2021, pp. 1–6.

[25] M. Di Renzo *et al.*, "Reconfigurable intelligent surfaces vs. relaying: Differences, similarities, and performance comparison," *IEEE Open J. Commun. Soc.*, vol. 1, pp. 798–807, Jun. 2020.

[26] W. Tang *et al.*, "Wireless communications with reconfigurable intelligent surface: Path loss modeling and experimental measurement," *IEEE Trans. Wireless Commun.*, vol. 20, no. 1, pp. 421–439, Jan. 2021.

[27] M. Di Renzo, F. Habibi Danufane, X. Xi, J. de Rosny, and S. Tretyakov, "Analytical modeling of the path-loss for reconfigurable intelligent surfaces – anomalous mirror or scatterer ?" in *Proc. IEEE SPAWC*, May 2020, pp. 1–5.

[28] H. Inaltekin, S. Atapattu, and J. S. Evans, "Optimum location-based relay selection in wireless networks," *IEEE Trans. Inform. Theory*, 2021, Early Access.

[29] A. A. Boulogeorgos and A. Alexiou, "Performance analysis of reconfigurable intelligent surface-assisted wireless systems and comparison with relaying," *IEEE Access*, vol. 8, pp. 94 463–94 483, May 2020.

[30] E. Basar, M. Di Renzo, J. De Rosny, M. Debbah, M.-S. Alouini, and R. Zhang, "Wireless communications through reconfigurable intelligent surfaces," *IEEE Access*, vol. 7, pp. 116 753–116 773, 2019.

[31] F. H. Danufane, M. D. Renzo, J. de Rosny, and S. Tretyakov, "On the path-loss of reconfigurable intelligent surfaces: An approach based on green's theorem applied to vector fields," *IEEE Trans. Commun.*, vol. 69, no. 8, pp. 5573–5592, 2021.

[32] Z.-Q. He and X. Yuan, "Cascaded channel estimation for large intelligent metasurface assisted massive mimo," *IEEE Wireless Commun. Lett.*, vol. 9, no. 2, pp. 210–214, 2020.

[33] S. Atapattu, R. Fan, P. Dharmawansa, G. Wang, J. Evans, and T. A. Tsiftsis, "Reconfigurable intelligent surface assisted two–way communications: Performance analysis and optimization," *IEEE Trans. Commun.*, vol. 68, no. 10, pp. 6552–6567, Oct. 2020.

[34] A. E. Canbilen, E. Basar, and S. S. Ikki, "Reconfigurable intelligent surface-assisted space shift keying," *IEEE Wireless Commun. Lett.*, vol. 9, no. 9, pp. 1495–1499, 2020.

[35] A. AlAmmouri, J. G. Andrews, and F. Baccelli, "SINR and throughput of dense cellular networks with stretched exponential path loss," *IEEE Trans. Wireless Commun.*, vol. 17, no. 2, pp. 1147–1160, Feb. 2018.

[36] Y. Fang, S. Atapattu, H. Inaltekin, and J. Evans, "Optimum reconfigurable intelligent surface selection for wireless networks," 2020. [Online]. Available: https://arxiv.org/abs/2012.11793

[37] J. F. C. Kingman, *Poisson Processes*. Oxford, UK: Clarendon Press, 1993.

[38] M. Abramowitz, *Handbook of Mathematical Functions, With Formulas, Graphs, and Mathematical Tables,*. New York, NY, USA: Dover Publications, Inc., 1974.

[39] I. S. Gradshteyn and I. M. Ryzhik, *Table of integrals, series, and products*, 7th ed. Amsterdam, Netherlands: Elsevier/Academic Press, 2007.

[40] A. Taha, M. Alrabeiah, and A. Alkhateeb, "Enabling large intelligent surfaces with compressive sensing and deep learning," *IEEE Access*, vol. 9, pp. 44 304–44 321, 2021.

[41] X. Guan, Q. Wu, and R. Zhang, "Anchor-assisted channel estimation for intelligent reflecting surface aided multiuser communication," *IEEE Trans. Wireless Commun.*, pp. 1–1, 2021.

[42] I. S. Gradshteyn and I. M. Ryzhik, *Table of Integrals, Series and Products*, 7th ed. Academic Press Inc, 2007.